Chapter 3:

Understanding the therapeutic potential of Kisspeptin-10 on Metastatic Suppression and EMT in Glioblastoma.

INTRODUCTION

Glioblastoma (GB) is among the most aggressive and fatal forms of primary brain tumors and is classified as grade IV astrocytoma by the World Health Organization. Despite significant advances in neurosurgical methods, radiation, and chemotherapy, GB remains an incurable disease in most patients, with a median survival rate of rarely exceeding 15 months. The ineffectiveness of conventional therapy is largely due to the highly invasive nature of GB, its molecular diversity, and a high level of resistance to apoptosis(Seker-Polat et al., 2022). The distinctive feature of GB is its ability to invade the surrounding normal brain parenchyma rather than developing well-defined borders. This feature of GB makes surgical resection ineffective and promotes rapid recurrence of the tumor. Unlike most peripheral cancers, GB is not known to metastasize systemically, but rather to invade widely in the brain by local invasion. This again emphasizes that invasion rather than proliferation alone is a key determinant of GB aggressiveness and clinical outcome (De Vleeschouwer, 2017). The distinctive feature of GB is its invasion of the surrounding normal brain parenchyma rather than developing well-defined borders. This feature of GB makes surgical resection ineffective and promotes rapid recurrence of the tumor. Unlike most peripheral cancers, GB is not known to metastasize systemically, but rather to invade widely in the brain by local invasion. This again emphasizes that invasion rather than proliferation alone is a key determinant of GB aggressiveness and clinical outcome.

The EMT-like transition in GB is associated with a high degree of reorganisation of cell-cell adhesion molecules, cytoskeletal elements, and transcriptional machinery. These changes result in reduced cell adhesion, enhanced migratory ability, and the ability of brain tumour cells to adapt dynamically to the brain microenvironment. It is pertinent to note that EMT-like changes are closely associated with resistance to treatment and tumour regrowth, underscoring their significance in cancer therapy(Falco et al., 2021). The invasion process in GB is mediated by the coordinated regulation of adhesion molecules and cytoskeletal elements, which together regulate cell migration and tissue invasion. In the current study, invasion behavior is analyzed using a selective group of regulators—CD44, β-catenin, Vimentin, E-cadherin, and N-cadherin—which are major molecular regulators of GB invasion. CD44 is a transmembrane adhesion receptor that mediates cell binding to extracellular matrix components (primarily hyaluronic acid, which is present in abundance in the brain microenvironment). High levels of CD44 expression also define the bulk of invasive GB cells, and are tightly linked with perivascular migration, stem-like characteristics, and resistance to therapy. Through cell–matrix interactions, CD44 contributes to the efficient migration of GB cells through the brain. β-catenin functions as both a structural part of adherens junction and a transcriptional modulator in the Wnt signalling pathway. Dysregulation of β-catenin leads to disruption of cell–cell adhesion and initiation of transcriptional programs that promote migration and invasion. In GB, abnormal β-catenin signalling has been associated

with increased invasiveness and with modified engagement with endothelial cells (Pearson & Regad, 2017).

Vimentin, the intermediate filament protein, is a key mesenchymal transition and cytoskeletal remodelling marker. Upregulation of vimentin makes cells more elastic and motile, facilitating the movement of GB cells through the dense extracellular matrix of brain. Thus, vimentin-regulated cytoskeletal plasticity is essential for invasive migration. E-cadherin is a classical adhesion molecule that maintains stable cell–cell junctions and suppresses migratory behaviour. Although GB cells are not epithelial, relative modulation of E-cadherin expression reflects changes in adhesion integrity. Loss or reduction of E-cadherin is associated with decreased cellular cohesion and increased invasion.

N-cadherin promotes cell motility and interaction with surrounding stromal and endothelial cells. Upregulation of N-cadherin facilitates invasive migration and vascular association, and the relative balance between E-cadherin and N-cadherin reflects a cadherin switch–like phenomenon that supports GB invasion. Together, dysregulation of these adhesion and cytoskeletal regulators constitutes a coordinated molecular program driving GB invasion (C. Guo et al., 2025).

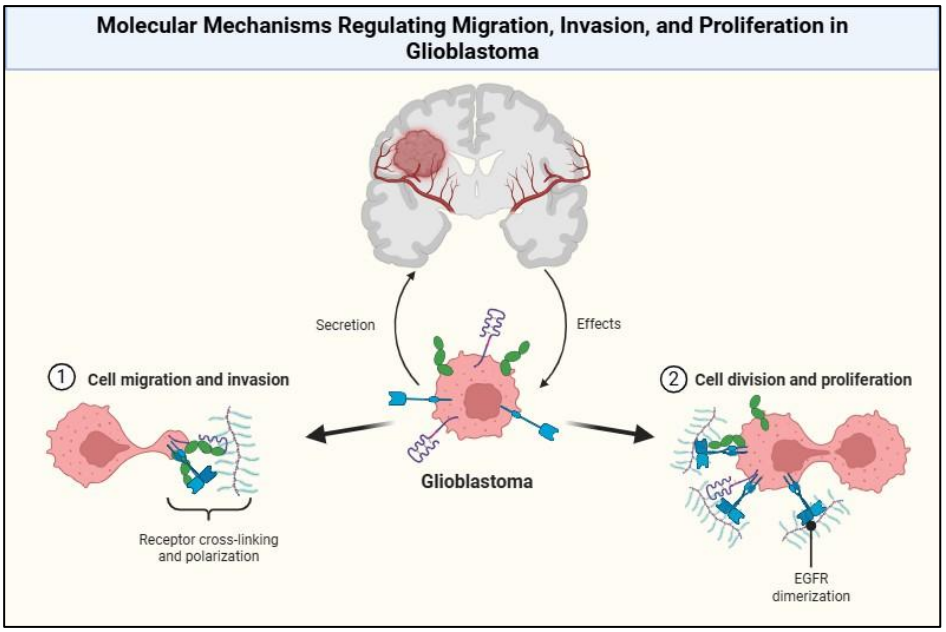

Figure 3.1: *Molecular mechanism regulating migration, invasion, and proliferation in Glioblastoma*

A distinctive mode of GB invasion is perivascular migration, also referred to as vascular co-option, wherein tumour cells migrate along existing blood vessels. This invasion strategy enables widespread tumour dissemination without dependence on classical angiogenesis. Adhesion molecules and EMT-like regulators play a pivotal role in mediating tumour–endothelial interactions during vascular invasion (Aum et al., 2014). Additionally, GB progression is tightly linked with disruption of the blood–brain

barrier (BBB), which is the result of breakdown of endothelial tight junctions and adhesion complexes. EMT-like transition and adhesion remodelling of GB cells lead to endothelial dysfunction, high vascular permeability, and an aberrant BBB. Disruption of the BBB facilitates not only tumour invasion but also inflammation, edema and therapy resistance, which add further challenges to the management of glioblastoma (Liu et al., 2019).

Figure 3.2: *Mechanism underlying with invasion in Glioblastoma*

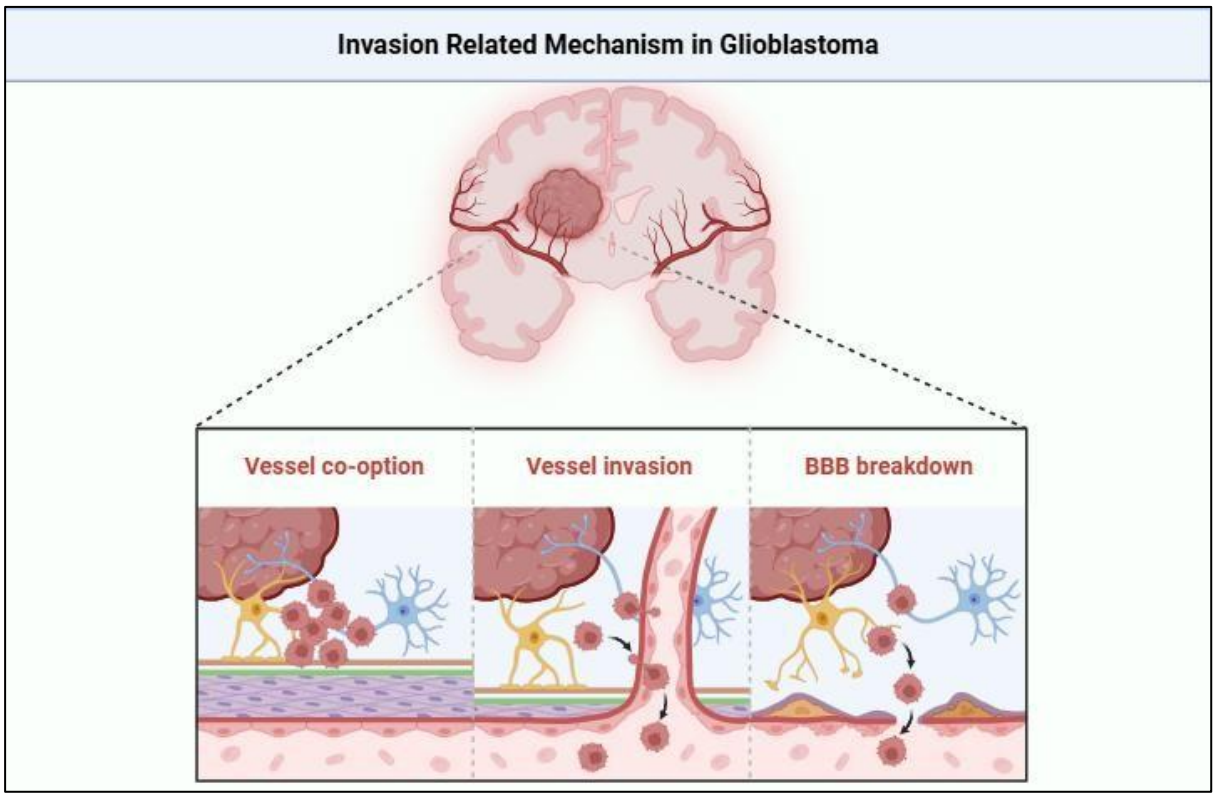

The invasive phenotype of GB is governed by extensive transcriptional reprogramming mediated by transcription factors and chromatin-modifying enzymes. These regulators coordinate the expression of genes involved in adhesion remodelling, cytoskeletal dynamics, EMT-like transition, and survival signalling.

At the same time, microRNAs (miRNAs) are post-transcriptional regulators that adjust gene expression by affecting the stability and translation of mRNAs. Aberrant expression of miRNAs in GB disturbs the regulatory equilibrium and drives invasive, mesenchymal features. Transcription factors and miRNAs interaction constitutes a multilevel regulatory network that maintains GB invasion and plasticity (Pouyan et al., 2025).

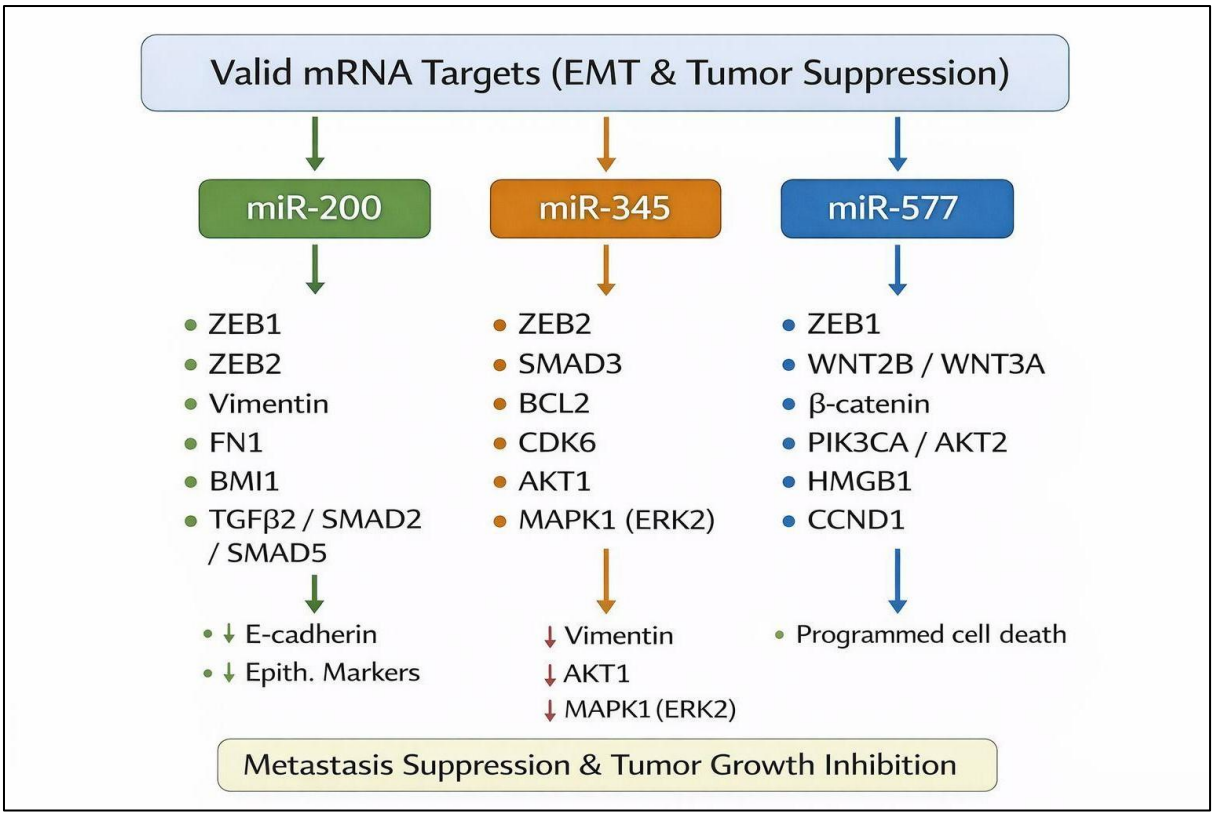

Figure 3.3: *Valid mRNA targets of the candidate miRNAs associated with Glioblastoma*

Several intracellular signalling pathways act as molecular hubs connecting extracellular information to the transcriptional and post-transcriptional regulation of invasion. Aberrant signalling pathways induce EMT-like transition, adhesion remodelling and apoptosis resistance. Continued engagement of pro-survival signals drives invasion and reduces sensitivity to standard treatments. Kisspeptin, encoded by the *KISS1* gene, was originally identified as a metastasis suppressor and later recognised for its essential role in reproductive endocrinology. Kisspeptin peptides exert their biological effects through binding to the *KISS1* receptor (*KISS1R/GPR54*), a G-protein-coupled receptor involved in diverse intracellular signalling cascades (Schweiger & Tannous, 2020; Tomikawa et al., 2012).

Beyond its endocrine function, the *KISS1/KISS1R* axis has been implicated in regulating cell migration, invasion, adhesion dynamics, transcriptional regulation, and apoptosis in multiple cancer types. Loss of *KISS1* expression has been correlated with increased tumour aggressiveness, whereas activation of Kisspeptin signalling has been shown to reduce invasive and metastatic traits. Despite growing evidence supporting the metastatic-suppressive role of Kisspeptin in cancer, its involvement in glioblastoma invasion, adhesion remodelling, vascular co-option, and BBB breakdown remains poorly understood. Given the central role of invasion in GB progression,

evaluating the effects of exogenous Kisspeptin-10 (Kp-10) provides a rational and targeted approach to investigate *KISS1/KISS1R* signalling in GB.

Exogenous Kp-10 allows direct activation of kisspeptin signalling and facilitates systematic evaluation of its effects on invasion-related adhesion regulators (CD44, β-catenin, Vimentin, E-cadherin, and N-cadherin), as well as upstream regulatory networks. Reduction of invasive phenotypes is also known to sensitise tumour cells to apoptosis, suggesting an integrated role for kisspeptin in invasion control and tumour cell elimination (Shah, Mohan, et al., 2025a). GB cells with invasive and mesenchymal features are also associated with antiapoptotic properties, which further promote treatment resistance. EMT-type conversion and adhesion remodelling result in activation of survival pathways that render tumour cells resistant to apoptosis. In contrast, re-establishment of adhesion homeostasis and inhibition of invasive signalling enhance pro-apoptotic responses (Shah et al., 2026).

Apoptosis in GB is predominantly mediated through the intrinsic mitochondrial pathway, involving key regulators such as BAX, BCL-2, Caspase-9, and Caspase-3. Evaluating apoptotic markers in conjunction with invasion-related regulators provides mechanistic insight into whether kisspeptin signalling can simultaneously inhibit invasion and promote apoptosis.

HYPOTHESIS

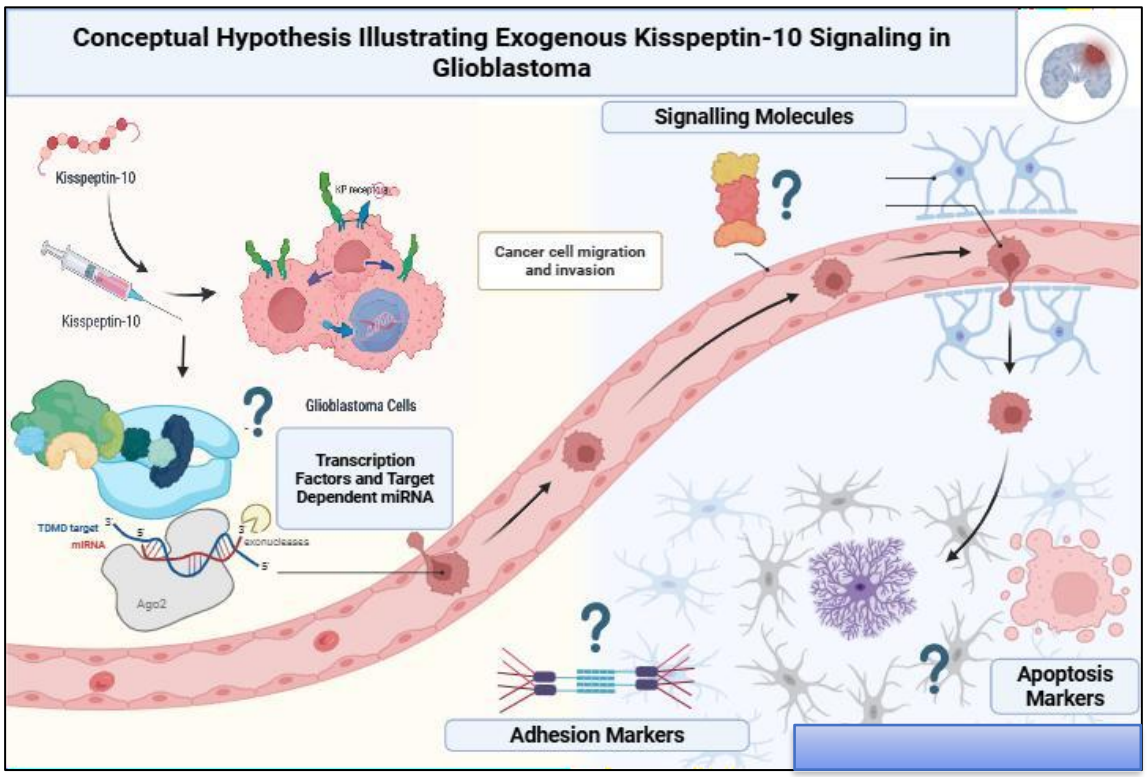

Figure 3.4: *Hypothesis illustrating the role of Kisspeptin-10 in Glioblastoma*

Exogenous administration of Kisspeptin-10 activates KISS1R-mediated signalling in glioblastoma cells, and may regulate EMT, adhesion dynamics, invasive potential, and apoptotic signalling pathways.

MATERIALS AND METHODS

3.3.1 Data Acquisition

The datasets of gene expression profiles were downloaded from the GEO database of the NCBI (https://www.ncbi.nlm.nih.gov/geo/). Two datasets, GDS3885 (Series Accession: GSE23806) - Expression profiling of 92 samples, including glioblastoma stem-like (GS) cell lines, corresponding primary tumours, and standard glioma cell lines, were utilized in this analysis. GDS3885 and GDS4473 were selected because they represent distinct GB biological contexts, enabling cross-dataset identification of robust, consistently dysregulated DEGs. In GDS3885, the control samples consist of non-tumour normal brain tissue. In GDS4473, control samples represent normal human astrocytes used as reference controls. The dataset was generated using the Affymetrix Human Genome U133 Plus 2.0 Array (GPL570) platform. GDS4473 (Series Accession: GSE31545) – Expression profiling of 14 samples, including glioma-propagating cells derived from oligodendroglial tumours and glioblastoma (GB). GDS3885 contains 22 GB samples and 8 non-tumour controls; GDS4473 includes 10 GB-propagating cells and 4 normal astrocyte controls. Because datasets were analysed independently rather than merged, batch correction was not required; instead, each dataset underwent separate RMA normalisation and probe collapsing. This dataset was also generated using the Affymetrix Human Genome U133 Plus 2.0 Array (GPL570) platform. Both raw CEL files were downloaded for preprocessing and analysis. Raw CEL files were processed using the 'affy' and 'limma' packages in R. Background correction and normalisation were performed using Robust Multi-array Average (RMA). Probe-to-gene mapping was carried out using the GPL annotation files, and probes mapping to the same gene were collapsed by median expression. A model matrix was constructed using model.matrix (~Condition), and contrasts were defined using make Contrasts (GB_vs_Control, levels = design) (Qian et al., 2023). Differential expression analysis was then performed with empirical Bayes moderation. The two datasets were analysed independently to avoid cross-platform batch effects. Therefore, harmonisation via ComBat was not applied. Each dataset underwent separate RMA normalisation, DEG extraction, and pathway analysis, followed by intersection-based integration of overlapping DEGs.

3.3.2 Differential Gene Expression Analysis

Differentially expressed genes (DEGs) between glioblastoma samples and normal brain controls were identified using the limma (v3.58.1) package. Genes with an adjusted p-value (FDR < 0.05) and absolute log2 fold-change ≥ 1 were considered significantly differentially expressed. Volcano plots and heatmaps were generated using the ggplot2 and pheatmap packages, respectively. DEGs were defined

as |log2FC| ≥ 1 with Benjamini–Hochberg FDR < 0.05. Upregulated genes were those with log2FC > 1 and downregulated with log2FC < –1.

3.3.3 UALCAN Analysis

To evaluate the clinical relevance and expression patterns of candidate genes, UALCAN (http://ualcan.path.uab.edu) was used. UALCAN is an interactive web-based resource for analysing cancer transcriptome data derived from The Cancer Genome Atlas (TCGA) and Clinical Proteomic Tumour Analysis Consortium (CPTAC) datasets.

3.3.4 Functional Enrichment Analysis

To explore the biological relevance of DEGs, Gene Ontology (GO) and Kyoto Encyclopedia of Genes and Genomes (KEGG) pathway analyses were performed using the clusterProfiler (v4.9.0) package and further using TNMPlot. TNMPlot was used to visually compare the expression of selected DEGs between tumour and normal brain tissues to cross-validate microarray findings. Terms with adjusted p-value < 0.05 were considered significantly enriched.

3.3.5 Protein–Protein Interaction (PPI) Network Construction

The DEGs were submitted to the STRING database (v11.5) to construct a protein–protein interaction (PPI) network. Interactions with a confidence score ≥ 0.7 were selected. STRING (v11.5) was queried using experimental, co-expression, curated database, and text-mining evidence with a confidence score ≥ 0.7. The network was visualised and analysed using Cytoscape (v3.9.1). Hub genes were identified using the cytoHubba plugin, employing degree, betweenness, and closeness centrality algorithms to prioritise genes with high network connectivity. Hub genes were ranked using Degree, MCC, and Betweenness centrality in cytoHubba. All hub-rank tables generated from cytoHubba. Gene-regulator networks were constructed using miRNet (v2.0), which applies integrated regulatory mapping from miRTarBase, TarBase, and TargetScan.

3.3.6 miRNA–mRNA Network Construction

To investigate post-transcriptional regulators of glioblastoma-associated DEGs, a miRNA–mRNA interaction network was constructed using miRNet 2.0 (https://www.mirnet.ca/). The DEG list was submitted as input to identify predicted and validated miRNA interactions. The resulting interaction data were imported into Cytoscape (v3.9.1) for visualisation and network analysis. In the network, DEGs were represented as blue nodes and interacting miRNAs as red nodes. Topological analysis identified candidate regulatory miRNAs, among which miR-200, miR-345, and miR-577 were prioritised based on connectivity and functional relevance. Further, the Gene-Regulator Network was constructed using Cytoscape v3.9.1 and RStudio (4.3.1). All analyses were performed in R v4.3.1. Data normality was assessed using the Shapiro–Wilk test prior to applying parametric or non-parametric statistics.

3.3.7 Cell Culture and Treatment

Human glioblastoma U87-MG cells were cultured in Dulbecco's Modified Eagle Medium (DMEM) supplemented with 10% fetal bovine serum (FBS) and 1% penicillin–streptomycin at 37 °C in a humidified atmosphere containing 5% CO_2. Cells were seeded at a density of 2×10^5 cells per well in six-well plates and allowed to adhere overnight. U87-MG cells were obtained from NCCS (National Centre for Cell Sciences, Pune) and do not require human/animal ethical clearance. U87-MG cells were authenticated by STR profiling and tested negative for mycoplasma contamination. Each experiment was performed with n = 3 biological replicates, each measured with 3 technical replicates.

Cell viability following Kisspeptin-10 treatment was evaluated using the MTT assay. U87MG cells were seeded into 96-well plates at a density of 5×10^3 cells per well and allowed to adhere overnight. Cells were then treated with increasing concentrations of Kisspeptin-10 ranging from 0, 10, 25, 50, 75, 100, 150, and 200 nM for 24 h. After treatment, 20 µL of MTT reagent (5 mg/mL in PBS) was added to each well and incubated for 4 h at 37 °C. The resulting formazan crystals were dissolved in 150 µL of DMSO, and absorbance was measured at 570 nm using a microplate reader. Cell viability (%) was calculated relative to untreated control wells. IC_{10} and IC_{50} values for Kisspeptin-10 and Doxorubicin were derived using nonlinear regression (four-parameter logistic model) fitted to MTT dose-response curves (GraphPad Prism 10).

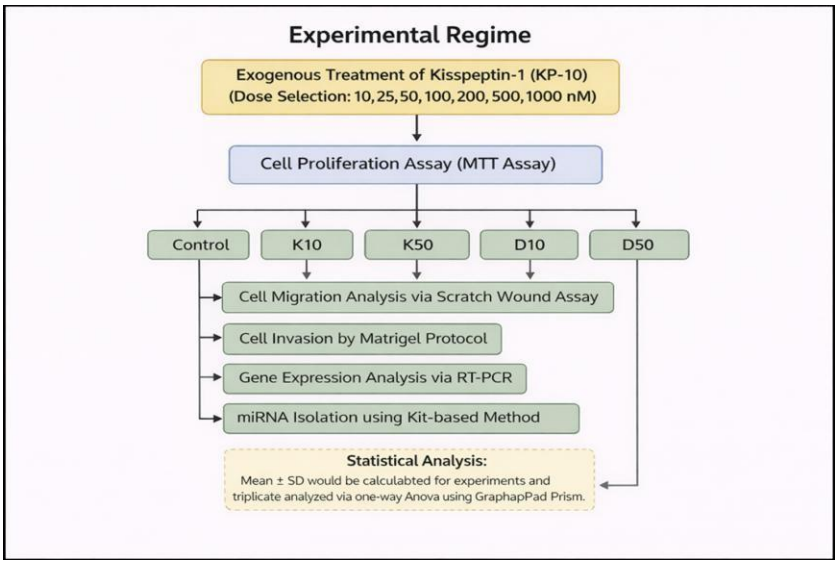

Figure 3.5: *Experimental Regime employed for U87MG cells.*

Treatments were divided into five groups:

- Control (untreated)
- Kisspeptin-10 at IC_{10} and IC_{50} concentrations: 10.13 nM (K10- IC_{10}) and 50.13 nM (K50- IC_{50})
- Doxorubicin at IC_{10} and IC_{50} concentrations: (positive control) at 78.31 nM (D10-IC10) and 151.2 nM (D50- IC_{50})

3.3.8 Cell Migration Assay

The protocol for U87MG cells was followed as mentioned in Chapter 2- 2.3.3.

3.3.9 Cell Invasion Assay

The protocol for U87MG cells was followed as mentioned in Chapter 2- 2.3.4.

3.3.10 miRNA Isolation and Quantitative Real-Time PCR (qPCR)

The protocol for U87MG cells was followed as mentioned in Chapter 2- 2.3.6.

3.3.11 Total RNA Isolation and cDNA Preparation Quantitative Real-Time PCR (qPCR)

The protocol for U87MG cells was followed as mentioned in Chapter 2- 2.3.5 for SP1, GATA2, CDX2, HDAC2, NMYC, FLI1, ZEB1, ECAD, NCAD, CD44, VIMENTIN, BCATENIN, CASPASE3, CASPASE8, CASPASE9, BAX, BCL2, PKA, PKR, PLCB1 and CJUN.

Statistical Analysis

The protocol for U87MG cells was followed as mentioned in Chapter 2- 2.3.7.

RESULTS

3.4.1. Identification of differentially expressed genes in glioblastoma

Comprehensive differential gene expression analysis across two independent GEO datasets revealed extensive transcriptional remodelling associated with glioblastoma (GB). In the GDS4473 dataset, which compared GB with anaplastic oligodendroglioma (AO), many genes were significantly dysregulated. Both upregulated and downregulated transcripts contributed to a broad $\log_2$ fold-change distribution. (Figure 3.5 a). The observed transcriptional changes encompassed genes involved in proliferation, invasion, cytoskeletal organisation, apoptosis, and metabolic regulation, highlighting disease-specific oncogenic and tumour-suppressive programs. This divergence supports the that GB represents a biologically distinct and more aggressive tumour entity relative to AO, characterised by heightened cellular plasticity and invasive potential.

In parallel, analysis of GDS3885, comparing GB tumour tissues with normal brain controls, revealed an even broader DEG landscape. Numerous genes exhibited extreme expression changes ($|\log_2 FC| > 4$) with strong statistical significance (adjusted $p < 0.001$), underscoring the magnitude of molecular reprogramming that accompanies malignant transformation (Figure 3.5 b).

a

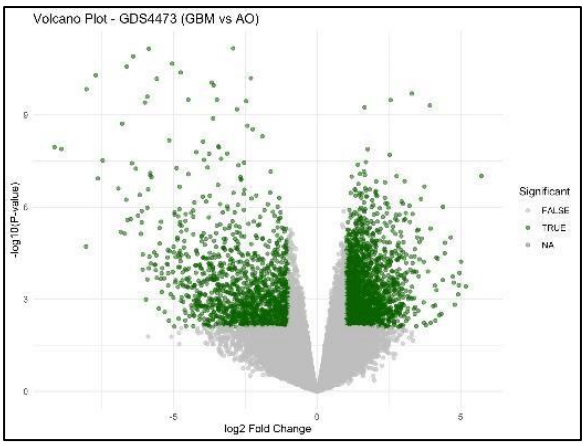

b

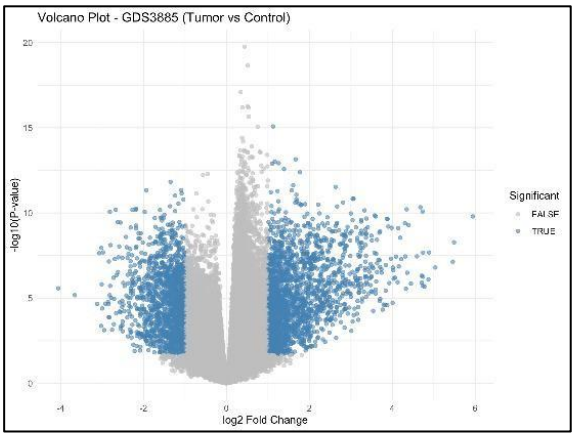

Figure 3.6: *(a) Volcano plot showcasing the $\log_2$ fold-change distribution for GDS4473 and (b) showcasing the $\log_2$ fold-change distribution for GDS3885.*

3.4.2. Overlap of differentially expressed genes across datasets

To identify robust and disease-consistent molecular signatures, DEGs from GDS4473 and GDS3885 were intersected. A total of **1401 genes** were commonly dysregulated across both datasets, defining a core GB transcriptomic signature independent of control tissue type. While GDS3885 contributed 8331 unique DEGs reflecting tumour–normal differences and GDS4473 contributed 3096 lineage-associated DEGs, the overlapping genes captured fundamental molecular programs intrinsic to Glioblastoma.

These shared DEGs are predicted to underpin critical hallmarks of glioblastoma, including enhanced invasion, angiogenesis, stem-like cell maintenance, metabolic reprogramming, and therapy resistance. Consequently, this gene set was selected for downstream functional enrichment, PPI network analysis, and regulatory modelling (Figure 3.6).

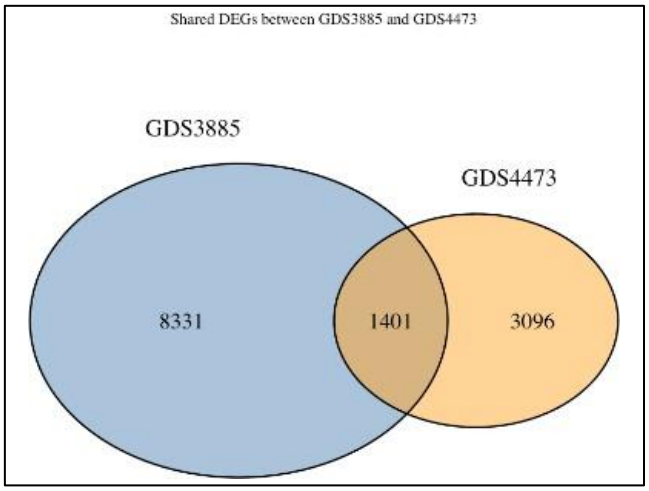

Figure 3.7: *Venn Diagram showcasing shared DEGs between GDS3885 and GDS4473*

3.4.3. Expression patterns of candidate genes in glioblastoma

Heatmap-based visualisation revealed distinct and coordinated expression patterns between normal brain tissues and GB samples. Several genes, including FAM107A, STARD10, SIK3, PAIP2, and SPRY2, were consistently upregulated across tumour samples, with fold changes ranging from ~4.5 to 8.9 relative to normal controls. Among these, FAM107A showed uniformly elevated expression across nearly all GB samples (Table 3.1).

In contrast, genes such as BIK, MSRB2, AGER, PDCL, ADD1, and OBSL1 were markedly downregulated, with expression levels reduced to ~0.7–0.9-fold relative to controls.

Notably, ANGPT1, CSF2RB, DAAM1, SAMD4A, and LSR displayed heterogeneous expression patterns, reflecting intratumoural heterogeneity (Figure 3.7).

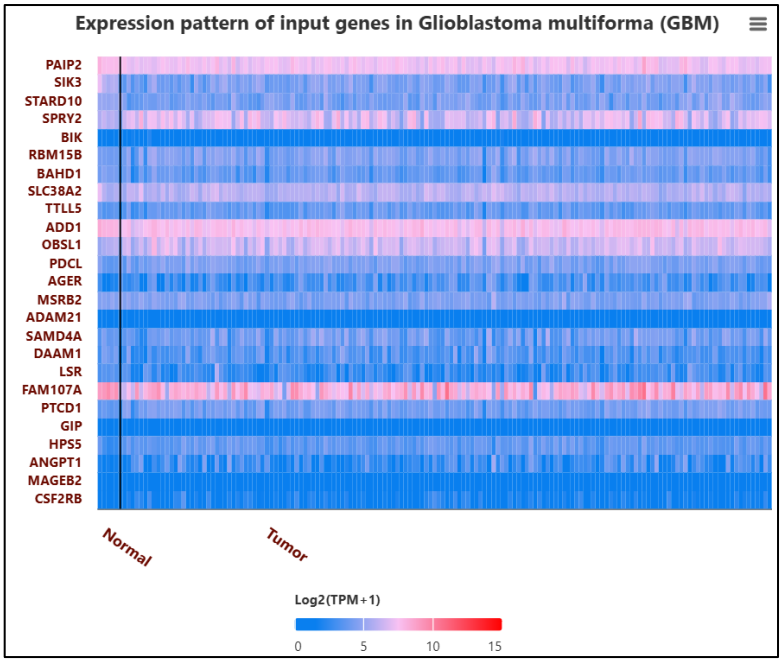

Figure 3.8: *Expression patterns of input genes in Glioblastoma*

Table 3.1: Functional Role and Clinical Implication of differentially expressed genes and their expression in Glioblastoma

Gene	Expression in GBM	Functional Role	Clinical / Translational Implication
FAM107A	Upregulated	Cytoskeletal regulation; glioma progression	Potential diagnostic marker and therapeutic target for invasion.
STARD10	Upregulated	Lipid transport & metabolism	May support metabolic reprogramming; candidate for metabolic targeting.
SIK3	Upregulated	Cell cycle & survival kinase	Possible drug target in kinase-inhibitor strategies.
PAIP2	Upregulated	Translation regulation	Enhances protein synthesis; role as proliferation marker.

SPRY2	Upregulated	RTK signalling modulation	Dual role in signalling; potential resistance mechanism.
BIK	Downregulated	Pro-apoptotic protein	Loss promotes therapy resistance; possible sensitisation target.
MSRB2	Downregulated	Antioxidant defence	Reduced oxidative repair; candidate for redox-based therapy.
AGER	Downregulated	Immune receptor & adhesion	Loss dampens immune responses; a biomarker of immune evasion.
ADD1	Downregulated	Cytoskeletal protein	Loss enhances invasion; a marker of structural deregulation.
ANGPT1	Heterogeneous	Angiogenesis regulation	Subtype-specific angiogenesis marker; possible anti-angiogenic target.
CSF2RB	Heterogeneous	Cytokine receptor signalling	Reflects microenvironmental diversity; immune-targeting candidate.
DAAM1	Heterogeneous	Actin cytoskeleton remodelling	Associated with invasion potential; a marker of migration heterogeneity.
LSR	Heterogeneous	Lipid metabolism & junctions	Potential stratifier for metabolic heterogeneity in GBM.

3.4.4. Protein–protein interaction (PPI) network construction and hub gene identification

PPI network construction using STRING revealed dense interconnectivity among shared DEGs (Figure 3.9), indicating strong functional coordination. Topological analysis identified CDK1, JUN, CDC20, ENO2, GNAS, TAGLN, FABP5, and RPL23 as central hub genes

These hubs showed marked upregulation in GB samples, with fold changes ranging from ~5.2 to 9.6. CDK1 and CDC20 are central regulators of mitotic progression, supporting uncontrolled proliferation. JUN integrates MAPK and stress-responsive signalling to promote tumorigenesis. Metabolic regulators ENO2 and FABP5 facilitate glycolytic and lipid metabolic reprogramming, essential for invasive tumour growth. Structural and translational regulators TAGLN and RPL23 highlight coordination between cytoskeletal dynamics and protein synthesis (Figure 3.8).

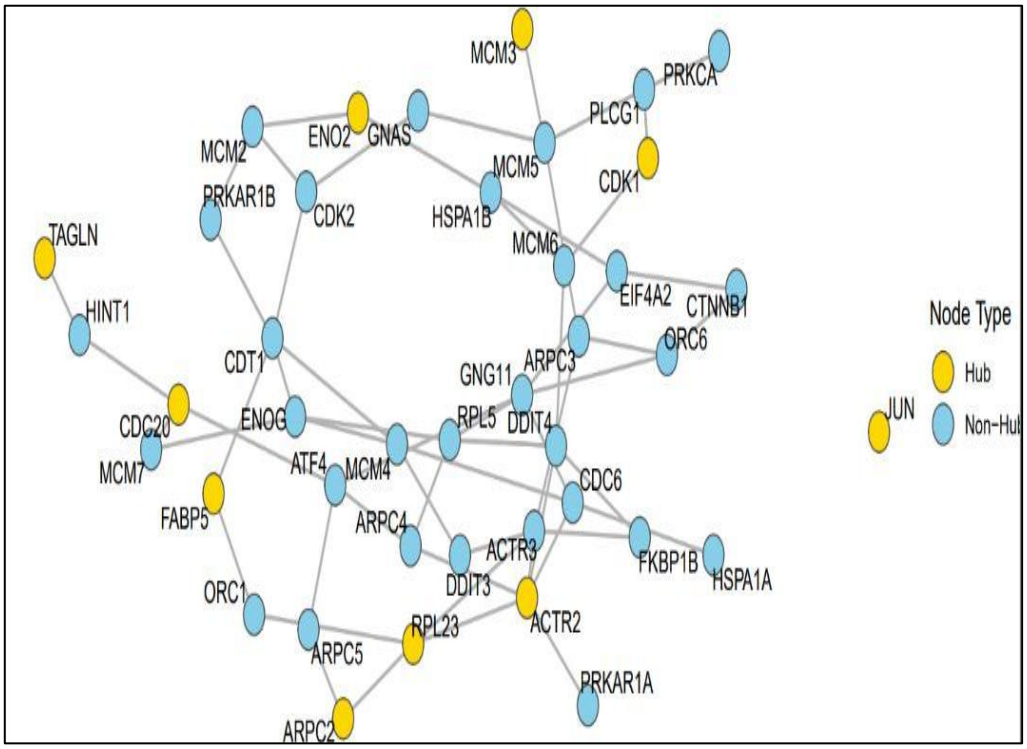

Figure 3.9: *Hub Gene Identification for Glioblastoma*

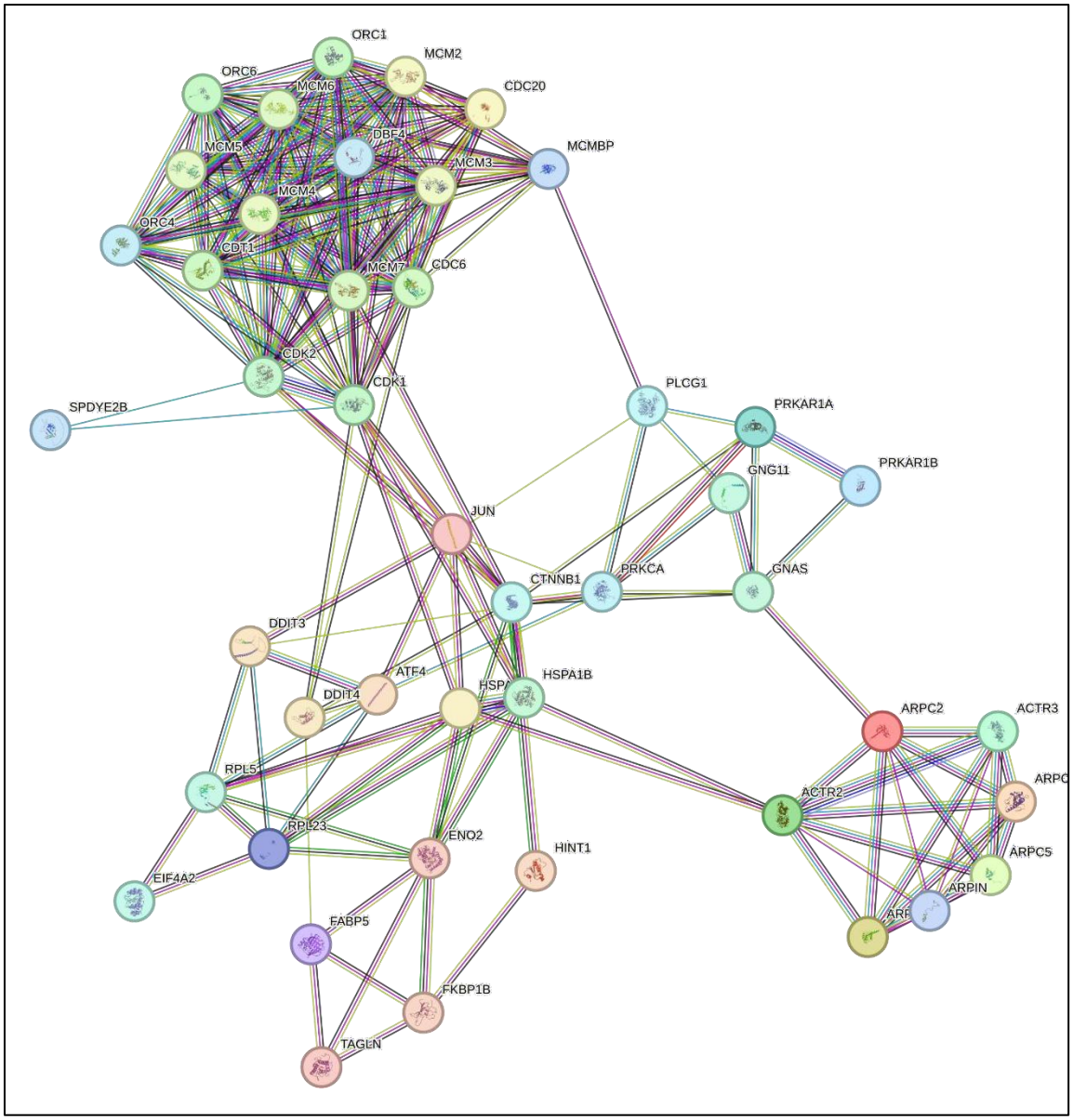

Figure 3.10: *Protein-Protein interaction via STRING for differentially expressed genes*

3.4.5. Gene Ontology (GO) enrichment analysis

GO enrichment analysis revealed significant involvement of DEGs in molecular functions such as zinc ion binding and transition metal ion binding, implicating metal-dependent enzymes in tumour progression. At the biological process level, proteolysis emerged as the dominant category consistent with enhanced invasion. Enrichment of ERK1/ERK2 signalling, developmental programs, and epigenetic regulation highlights proliferative and adaptive mechanisms. Cellular component analysis showed enrichment in cytoskeleton, actin cytoskeleton, RNA methyltransferase complexes, cell–cell junctions, and death-inducing signalling complexes (Figure 3.10).

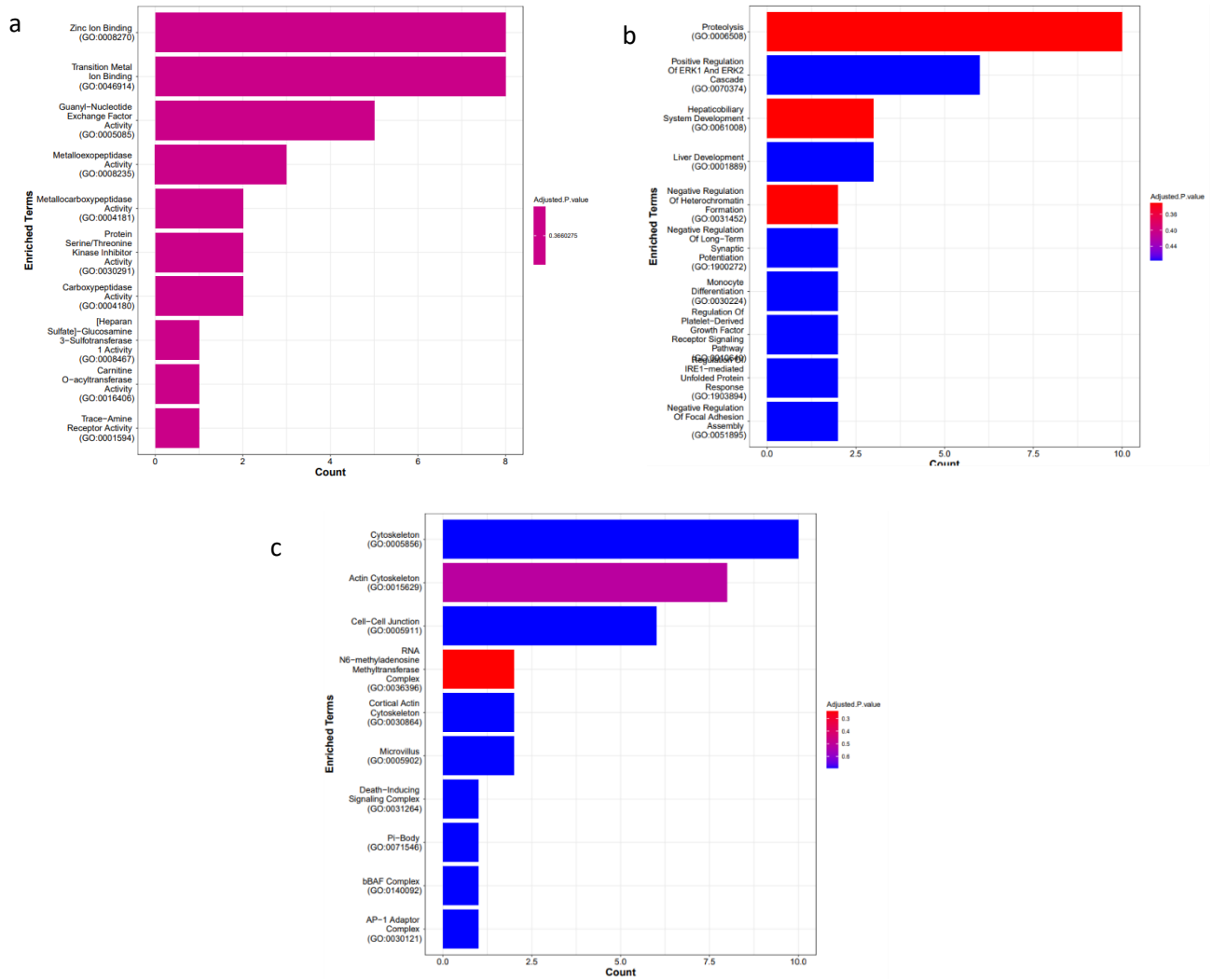

Figure 3.11: *Gene Ontology enrichment analysis showcasing (a) Molecular Function, (b) Cellular process and (c) Cellular component.*

Table 3.2: Gene Ontology description along with P-values for differentially expressed genes for Glioblastoma

Ontology	ID	Description	Count	P-value	Adjusted P-value
MF	GO:0008270	Zinc ion binding	8	0.0025	0.3660
MF	GO:0046914	Transition metal ion binding	8	0.0028	0.3660
MF	GO:0005085	Guanyl-nucleotide exchange factor activity	5	0.0041	0.3660
MF	GO:0008235	Metallopeptidase activity	4	0.0062	0.3660

MF	GO:0004181	Metallocarboxypeptidase activity	3	0.0085	0.3660
MF	GO:0032571	Protein serine/threonine kinase inhibitor	3	0.0094	0.3660
MF	GO:0004180	Carboxypeptidase activity	3	0.0101	0.3660
MF	GO:0008467	Heparan sulfated-glucosamine 3-sulfotransferase 1 activity	2	0.0148	0.3660
MF	GO:0016406	Carnitine O-acyltransferase activity	2	0.0171	0.3660
MF	GO:0001594	Trace-amine receptor activity	2	0.0184	0.3660
BP	GO:0006508	Proteolysis	9	0.0015	0.3600
BP	GO:0070374	Positive regulation of ERK1 and ERK2 cascade	6	0.0022	0.4000
BP	GO:0061008	Hepatobiliary system development	3	0.0034	0.4200
BP	GO:0001889	Liver development	3	0.0042	0.4200
BP	GO:0031452	Negative regulation of heterochromatin formation	2	0.0056	0.4400
BP	GO:1900272	Negative regulation of long-term synaptic potentiation	2	0.0062	0.4400
BP	GO:0030224	Monocyte differentiation	2	0.0071	0.4400
BP	GO:1903849	IRE1-mediated unfolded protein response	2	0.0082	0.4400
BP	GO:0051895	Negative regulation of focal adhesion assembly	2	0.0091	0.4400
CC	GO:0005856	Cytoskeleton	9	0.0019	0.6000
CC	GO:0015629	Actin cytoskeleton	8	0.0025	0.5600
CC	GO:0005911	Cell-cell junction	6	0.0044	0.6000

CC	GO:0036396	N6-methyladenosine methyltransferase complex	2	0.0059	0.3000
CC	GO:0030864	Cortical actin cytoskeleton	3	0.0068	0.6000
CC	GO:0005902	Microvillus	3	0.0072	0.6000
CC	GO:0031264	Death-inducing signalling complex	2	0.0087	0.6000
CC	GO:0071546	P-body	2	0.0092	0.6000
CC	GO:0140092	bBAF complex	2	0.0104	0.6000
CC	GO:0030121	AP-1 adaptor complex	2	0.0111	0.6000

3.4.6 Gene–regulator association network reveals coordinated control of invasion, EMT, and apoptosis in glioblastoma

To further delineate the regulatory architecture underlying glioblastoma-associated transcriptional reprogramming, an extended gene–regulator association network was constructed and visualised. The network integrates transcriptional regulators (yellow nodes) with their downstream target genes (green nodes), where node size reflects degree centrality and edges denote regulatory associations. The resulting network exhibits a modular yet highly interconnected topology, highlighting coordinated regulation of invasion, epithelial–mesenchymal transition (EMT), cytoskeletal dynamics, angiogenesis, and apoptotic signalling (Figure 3.11).

- **Identification of key regulatory hubs**

Several regulators emerged as prominent hubs with high degree centrality, indicating their central role in coordinating gene expression programs in glioblastoma. Among these, ZEB1, CDH2, CD44, CTNNB1, VIM, and MMP2 represented the most interconnected nodes within the network. ZEB1 occupied a central position linking multiple EMT-associated genes, including SNAI1, SNAI2, FOXC2, SPRY2, and SAMD4A, suggesting its role as a master transcriptional repressor orchestrating mesenchymal transition. Similarly, CDH2 (N-cadherin) and VIM (Vimentin) formed dense interaction clusters with integrins (ITGA5, ITGB1), focal adhesion components (PXN, PTK2), and Rho GTPase signalling molecules (RHOA, RAC1, RHOC).

- **Invasion and extracellular matrix remodelling module**

A distinct invasion-centric module was characterised by strong connectivity among MMP2, MMP9, FN1, VCAN, COL1A1, COL1A2, COL5A1, and COL5A2, reflecting active extracellular matrix degradation and structural remodelling. MMP2 emerged as a highly connected node bridging ECM components with EMT regulators. Angiogenesis-related genes, including VEGFA, ANGPT1, and TGFβ1/TGFβR2, were closely associated with this module, suggesting coupling between invasive behaviour and vascular remodelling. The presence of COL1A1/2 and COL5A1/2 further indicates stromal interaction and tumour–microenvironment crosstalk as integral components of glioblastoma progression.

- **Adhesion and cytoskeletal signalling axis**

The network revealed a tightly interconnected adhesion and cytoskeletal signalling axis centred around CD44, LAMC2, ITGA5, ITGB1, PXN, and CDK6. These genes collectively regulate focal adhesion turnover, mechano-transduction, and cell motility. Notably, DAAM1 and RHO-family GTPases formed a subnetwork linking actin cytoskeletal reorganisation to EMT progression. A separate but connected module comprised apoptosis-associated genes, including BAX, BIK, CASP3, CASP8, CASP9, and BCL2. Within this cluster, BCL2 functioned as a central survival regulator, interacting with multiple pro-apoptotic effectors. Interestingly, this apoptosis module was connected to EMT and adhesion nodes through AGER, LSR, and OBSL1.

- **Transcriptional and signalling regulators**

Upstream transcriptional regulators such as SOX2, STAT3, SP1, NFκB, and TP53 were positioned at the periphery of the network but maintained multiple downstream connections, indicating their role in global transcriptional control rather than pathway-specific regulation. SOX2 and STAT3, in particular, linked stemness-associated signalling with EMT and invasion modules.Growth factor receptors and signalling mediators, including EGFR, PDGFRA, MET, and TGFβ signalling components, were also embedded within the network, connecting extracellular cues to intracellular transcriptional and cytoskeletal responses.

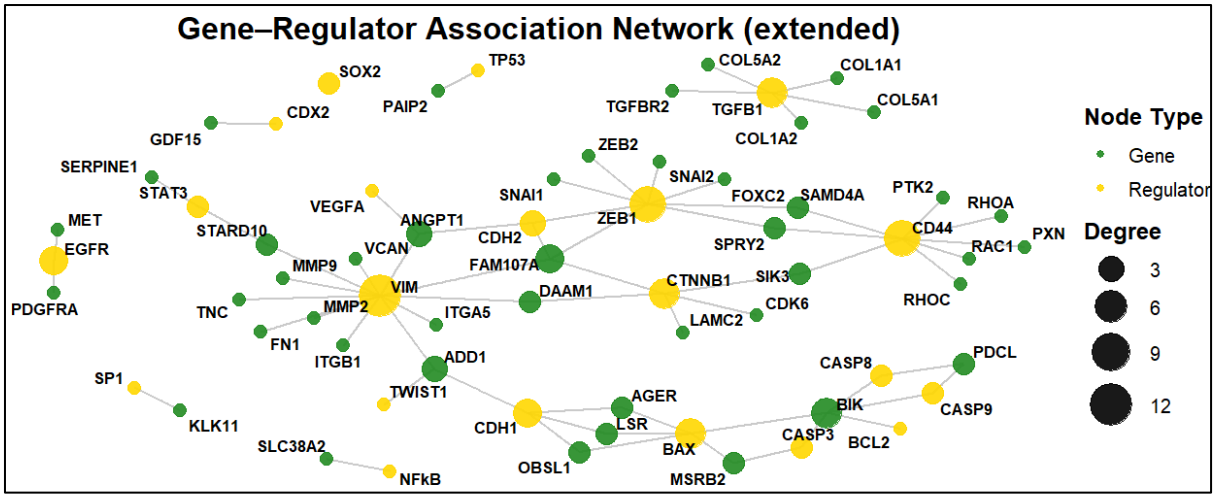

Figure 3.12: *Gene Regulatory Network for differentially expressed genes*

3.4.7 Kisspeptin-10 Exhibits Dose-Dependent Cytotoxicity in U87MG Cells

The cytotoxic effects of Kisspeptin-10 on U87MG glioblastoma cells were evaluated using the MTT assay across a range of concentrations. Kisspeptin-10 treatment resulted in a clear dose-dependent reduction in cell viability, indicating potent growth-inhibitory activity (Figure 3.12). These results demonstrate that Kisspeptin-10 exerts cytotoxic effects at nanomolar concentrations in glioblastoma cells, with an IC_{50} value of 50.13 nM. Based on these findings, the IC_{10} dose (10.13 nM; K10) was selected for subsequent migration and invasion assays to assess non-lethal effects, while the IC_{50} dose (50.13 nM; K50) was used for molecular assays to evaluate moderately cytotoxic effects.

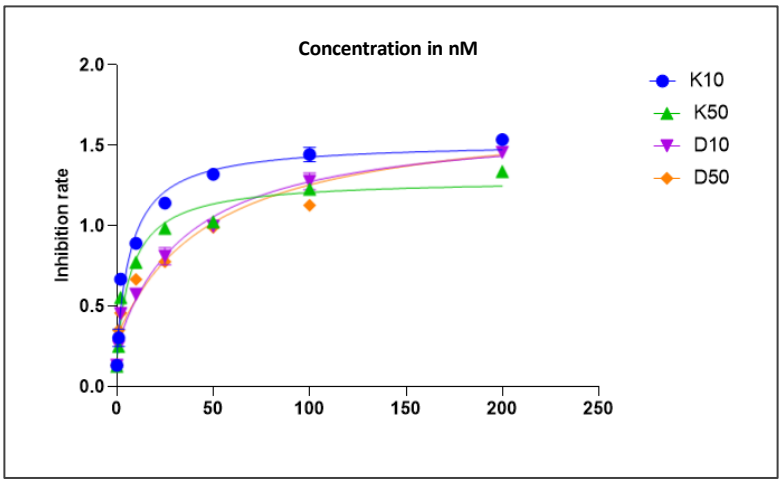

Figure 3.13: *Cell Cytotoxicity assay for U87 MG cells*

3.4.8 Kisspeptin-10 Inhibits Migratory Potential of U87MG Cells

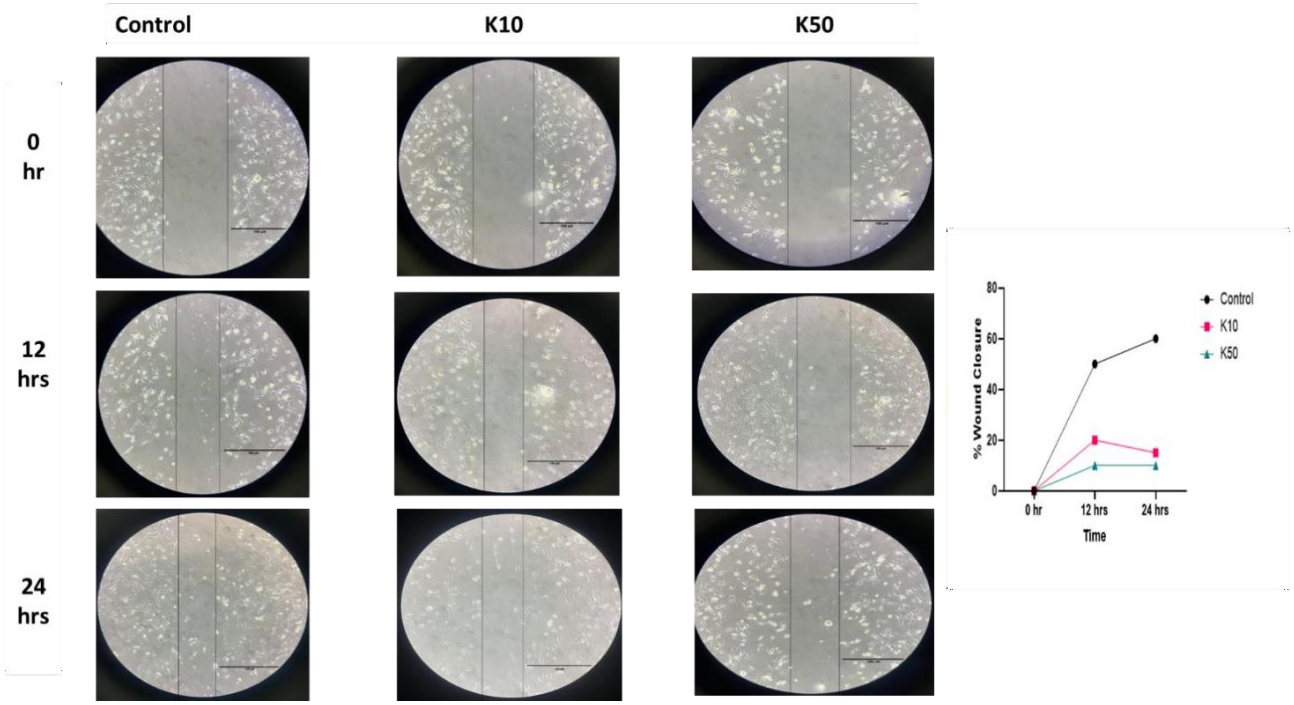

Figure 3.14a: *Cell invasion assay for U87 MG cells (Scale bar indicates 100 µM)*

3.4.9 Kisspeptin-10 Reduces Invasive Potential of U87MG Cells

The effect of Kisspeptin-10 on glioblastoma cell invasion was further examined using a Matrigel-coated trans-well invasion assay. Treatment with Kisspeptin-10 resulted in a significant reduction in the number of invading cells. Both K10- and K50-treated groups exhibited markedly decreased invasion compared to the control group, with the most substantial inhibition observed in the K50 group.

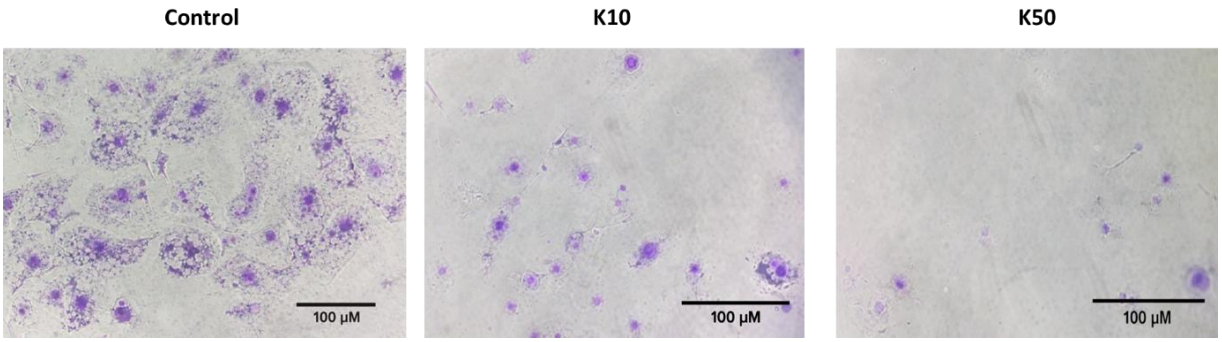

Figure 3.14b: *Cell invasion assay for U87 MG cells*

3.4.10 Consolidated Gene Expression Analysis Reveals Coordinated Molecular Reprogramming by Kisspeptin-10

Table 3.3: NanoDrop spectrophotometric analysis of total RNA isolated from U87MG cells

Sample	**260/280 Ratio**	**260/230 Ratio**	**RNA Concentration (ng/µL)**
Control	2.06	2.15	574.62
K10	2.04	2.10	436.81
K50	2.02	2.07	368.47
D10	2.05	2.12	402.95
D50	2.03	2.08	341.26

Quantitative real-time PCR analysis showed that ECAD expression was significantly increased following Kisspeptin-10 treatment at K10 (2.78 ± 0.18, $p < 0.01$) and K50 (5.94 ± 0.31, $p < 0.001$), while doxorubicin treatment also resulted in significant upregulation at D10 (2.31 ± 0.17, $p < 0.01$) and D50 (2.35 ± 0.28, $p < 0.01$). β-catenin expression was significantly elevated at K10 (2.53 ± 0.16, $p < 0.01$) and K50 (5.21 ± 0.29, $p < 0.001$), whereas changes observed with doxorubicin were not statistically significant. NCAD expression was significantly reduced at K10 (0.88 ± 0.06, $p < 0.05$) and K50 (0.72 ± 0.04, $p < 0.01$). Vimentin expression was significantly downregulated at K50 (0.71 ± 0.04, $p < 0.01$), and CD44 expression was significantly decreased at K10 (0.89 ± 0.05, $p < 0.05$) and K50 (0.83 ± 0.04, $p < 0.01$), with further reduction at D50 (0.76 ± 0.04, $p < 0.01$). (Standard curves as indicated in Appendix 1)

Among apoptosis-related genes, BAX expression was significantly increased at K10 (3.24 ± 0.05, $p < 0.001$) and K50 (6.82 ± 0.05, $p < 0.001$), while doxorubicin induced lower but significant increases at D10 (1.61 ± 0.04, $p < 0.05$) and D50 (1.71 ± 0.07, $p < 0.05$). CASP3 expression was significantly elevated at K10 (3.91 ± 0.25, $p < 0.001$) and K50 (7.54 ± 0.41, $p < 0.001$), with strong induction also observed at D50 (8.21 ± 0.45, $p < 0.001$). CASP9 expression showed significant upregulation at K10 (3.47 ± 0.22, $p < 0.001$), K50 (6.88 ± 0.06, $p < 0.001$), and D50 (7.79 ± 0.39, $p < 0.001$). BCL2 expression was significantly reduced at K50 (0.50 ± 0.03, $p < 0.001$), while CASP8 showed a mild but significant reduction at K50 (0.84 ± 0.04, $p < 0.05$). Analysis of transcription factors indicated that HDAC2 expression was significantly downregulated at K10 (0.88 ± 0.05, $p < 0.05$) and K50 (0.45 ± 0.04, $p < 0.001$). GATA2 expression was significantly increased at K10 (3.42 ± 0.09, $p < 0.001$) and markedly elevated at K50 (10.98 ± 0.05, $p < 0.001$). CDX2 expression was significantly upregulated at

K10 (3.12 ± 0.02, $p < 0.001$) and K50 (6.37 ± 0.04, $p < 0.001$). FLI1 expression was significantly reduced at K10 (0.81 ± 0.05, $p < 0.05$) and K50 (0.33 ± 0.04, $p < 0.001$). SP1 expression showed significant upregulation at K10 (1.91 ± 0.05, $p < 0.01$) and K50 (3.31 ± 0.04, $p < 0.001$), while NMYC expression was significantly reduced at K50 (0.79 ± 0.04, $p < 0.05$). ZEB1 expression was significantly downregulated at K10 (0.89 ± 0.05, $p < 0.05$) and K50 (0.61 ± 0.04, $p < 0.001$). Among signaling molecules, PKA expression was significantly increased at K10 (2.87 ± 0.09, $p < 0.001$) and K50 (5.63 ± 0.04, $p < 0.001$), while PKR (EIF2AK2) expression showed significant upregulation at K10 (3.41 ± 0.03, $p < 0.001$) and K50 (6.74 ± 0.02, $p < 0.001$). PLCB1 expression was significantly elevated at K10 (2.58 ± 0.08, $p < 0.01$) and K50 (2.59 ± 0.03, $p < 0.01$), with a higher increase observed at D50 (4.82
± 0.09, $p < 0.001$). JUN expression was significantly reduced at K10 (0.90 ± 0.05, $p < 0.05$) and K50 (0.72 ± 0.04, $p < 0.01$).

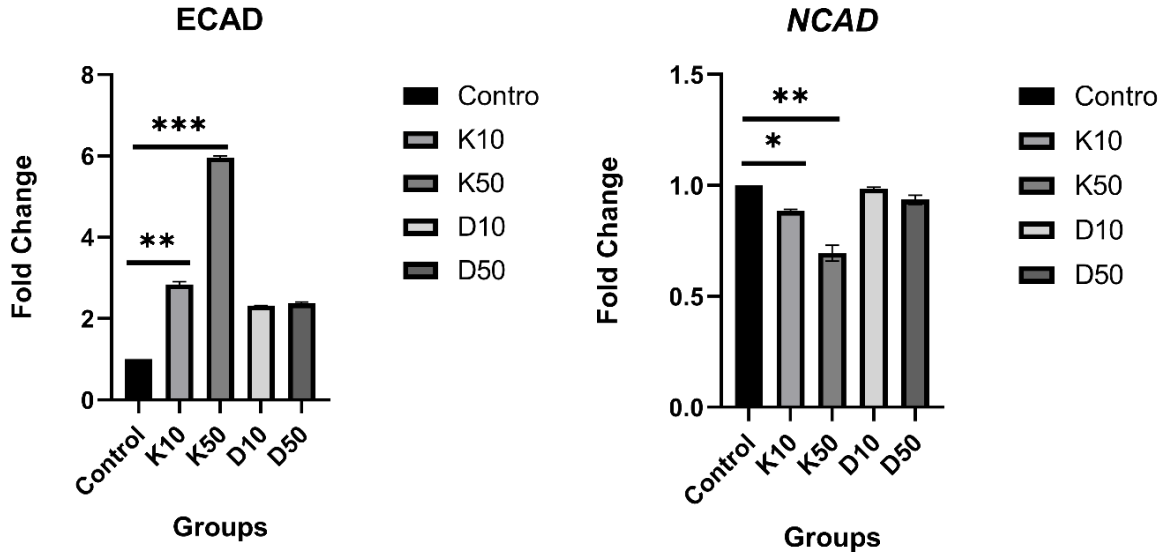

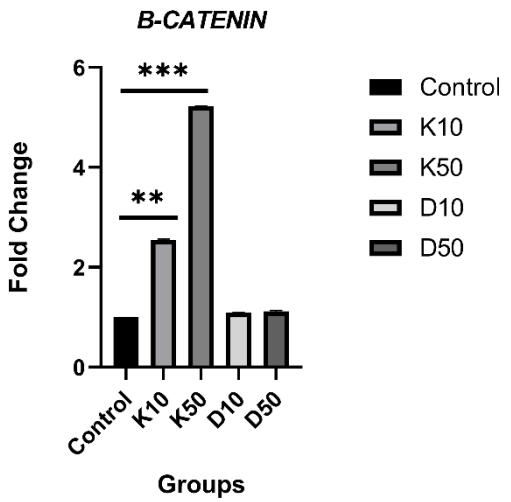
B-CATENIN
Fold Change
6
4
2
0
***
**
Control
K10
K50
D10
D50
Control
K10
K50
D10
D50
Groups

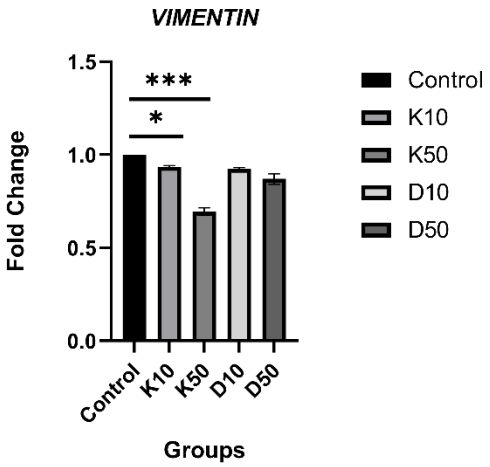
VIMENTIN
Fold Change
1.5
1.0
0.5
0.0
***
*
Control
K10
K50
D10
D50
Control
K10
K50
D10
D50
Groups

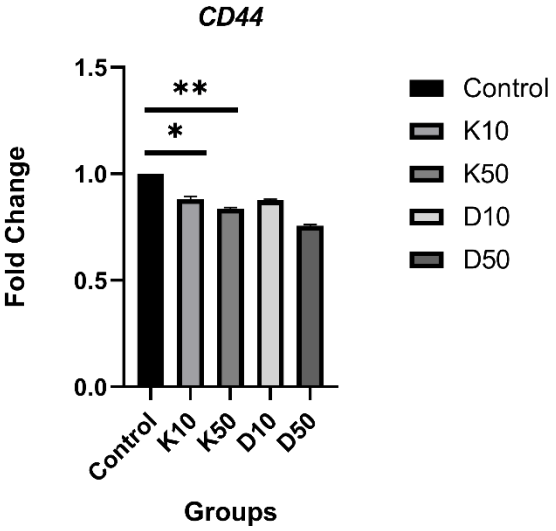
CD44
Fold Change
1.5
1.0
0.5
0.0
**
*
Control
K10
K50
D10
D50
Control
K10
K50
D10
D50
Groups

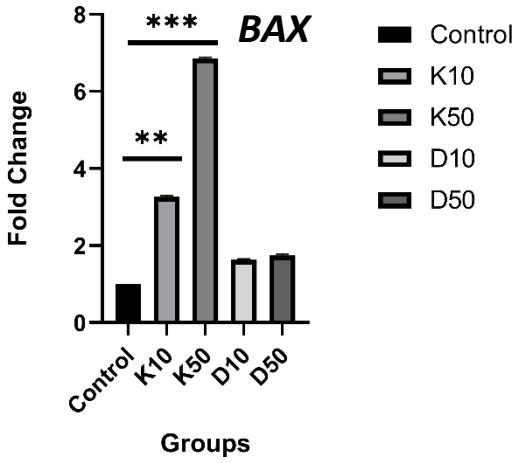
BAX
***
**
Fold Change
Groups
Control
K10
K50
D10
D50

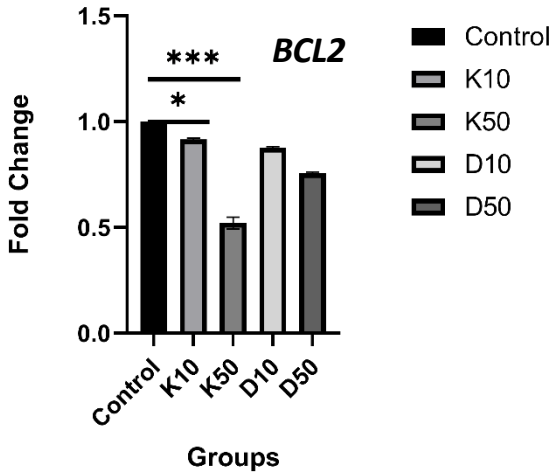
BCL2
***
*
Fold Change
Groups
Control
K10
K50
D10
D50

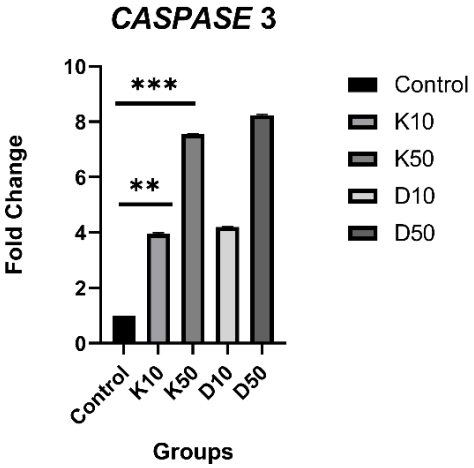
CASPASE 3
***
**
Fold Change
Groups
Control
K10
K50
D10
D50

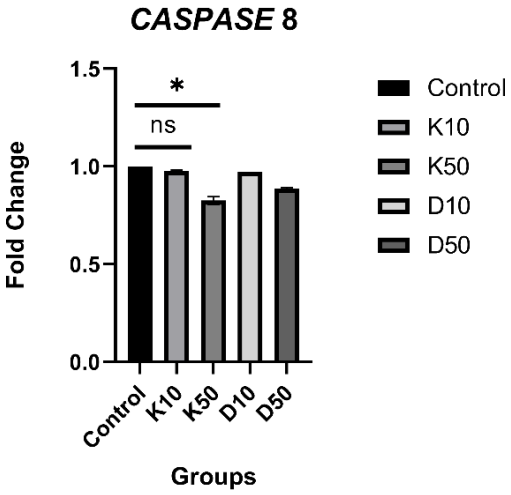
CASPASE 8
*
ns
Fold Change
Groups
Control
K10
K50
D10
D50

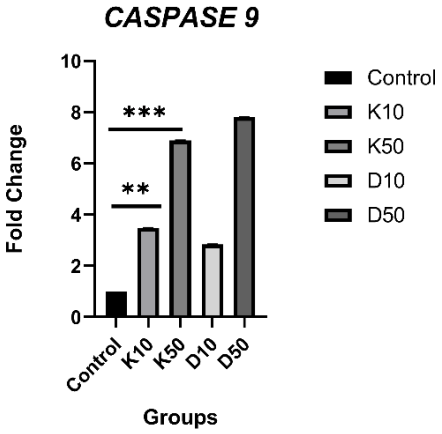
CASPASE 9
***
**
Fold Change
Groups
Control
K10
K50
D10
D50

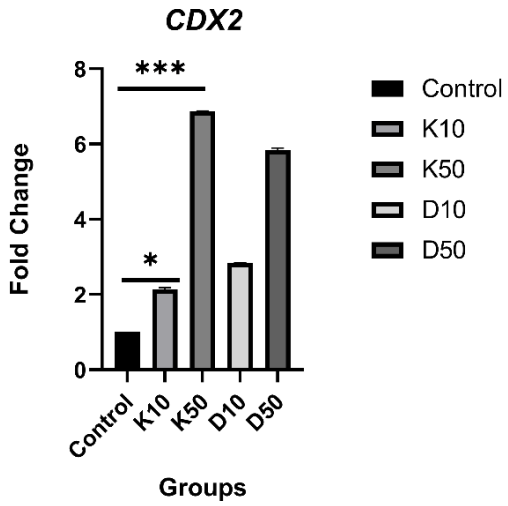
CDX2
Fold Change
8
6
4
2
0
***
*
Control
K10
K50
D10
D50
Control
K10
K50
D10
D50
Groups

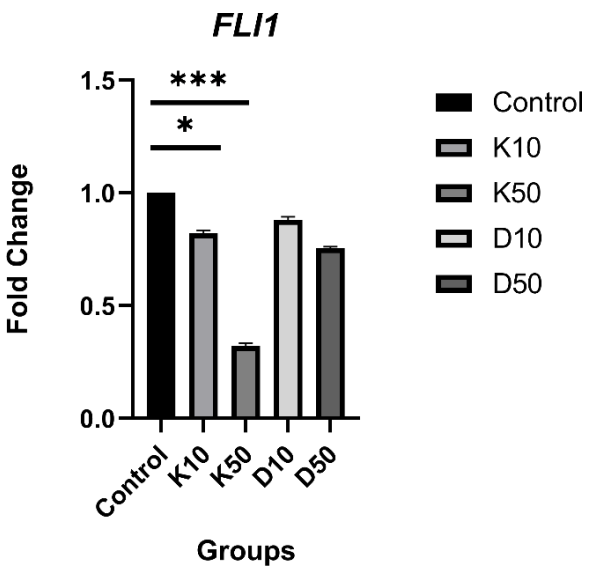
FLI1
Fold Change
1.5
1.0
0.5
0.0
***
*
Control
K10
K50
D10
D50
Control
K10
K50
D10
D50
Groups

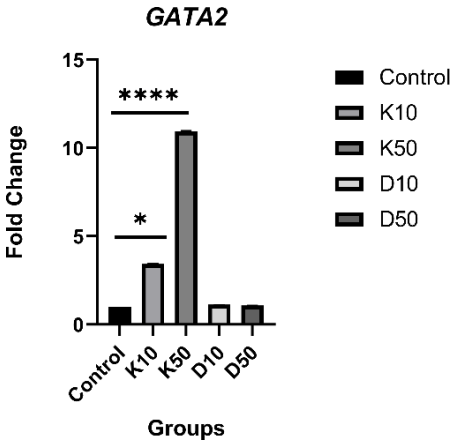
GATA2
Fold Change
15
10
5
0
****
*
Control
K10
K50
D10
D50
Control
K10
K50
D10
D50
Groups

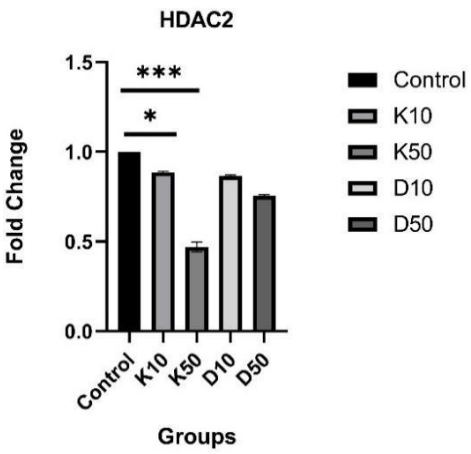
HDAC2
Fold Change
1.5
1.0
0.5
0.0
***
*
Control
K10
K50
D10
D50
Control
K10
K50
D10
D50
Groups

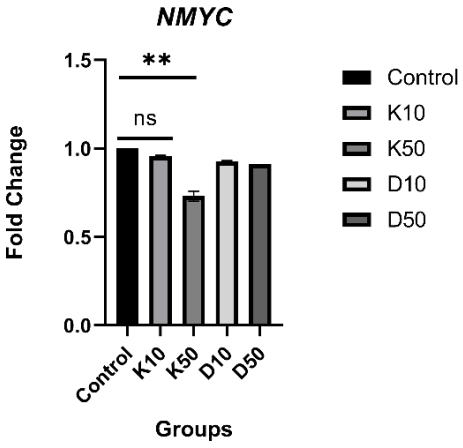
NMYC
Fold Change
1.5
1.0
0.5
0.0
**
ns
Control
K10
K50
D10
D50
Control
K10
K50
D10
D50
Groups

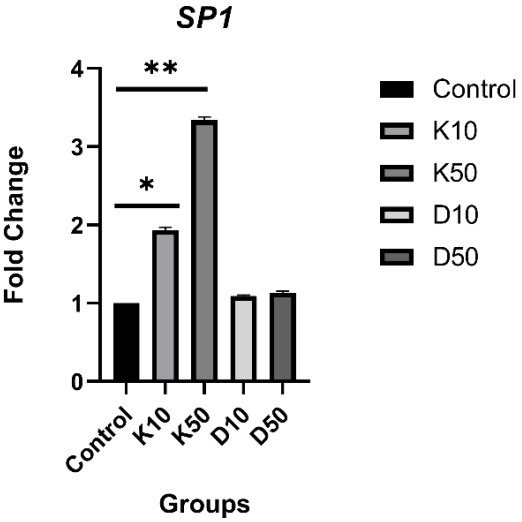
SP1
Fold Change
4
3
2
1
0
**
*
Control
K10
K50
D10
D50
Control
K10
K50
D10
D50
Groups

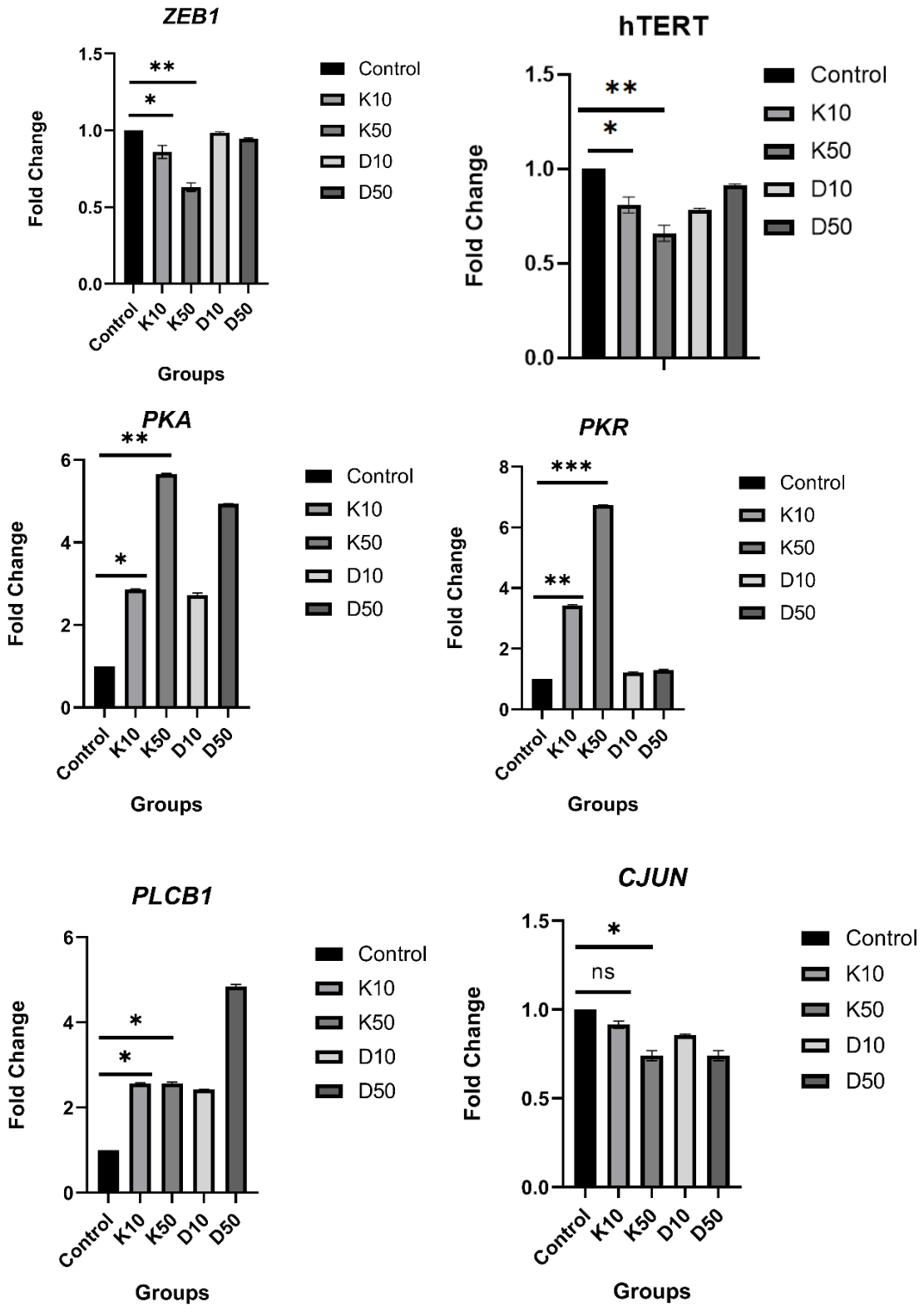

Figure 3.15: *Gene Expression analysis of Transcription factors, Adhesion markers, Apoptosis markers and Signalling molecules for U87 MG cells.*

Table 3.4: Consolidated Gene Expression profiles of Transcription factors, Adhesion markers, Apoptosis markers and Signalling molecules for U87 MG cells.

Category	Gene	Control	K10	K50	D10	D50
EMT / Adhesion	ECAD	1.00	2.78± 0.18	5.94± 0.31	2.31± 0.17	2.35± 0.28
	B-CATENIN	1.00	2.53± 0.16	5.21 ± 0.29	1.08± 0.15	1.09± 0.12
	NCAD	1.00	0.88± 0.06	0.72± 0.04	0.92± 0.05	0.89± 0.04
	VIM	1.00	0.94± 0.05	0.71± 0.04	0.83± 0.05	0.74± 0.04
	CD44	1.00	0.89± 0.05	0.83± 0.04	0.87± 0.05	0.76± 0.04
Apoptosis	BAX	1.00	3.24± 0.05	6.82± 0.05	1.61± 0.04	1.71± 0.07
	CASP3	1.00	3.91± 0.25	7.54± 0.41	4.18± 0.27	8.21± 0.45
	CASP9	1.00	3.47± 0.22	6.88± 0.06	2.82± 0.25	7.79± 0.39
	BCL2	1.00	0.91± 0.04	0.50± 0.03	0.86± 0.04	0.75± 0.04
	CASP8	1.00	0.98± 0.05	0.84± 0.04	0.91± 0.05	0.89± 0.04
Transcription Factors	HDAC2	1.00	0.88± 0.05	0.45± 0.04	0.84± 0.05	0.76± 0.04
	GATA2	1.00	3.42± 0.09	10.98± 0.05	1.12± 0.02	1.08± 0.01
	CDX2	1.00	3.12± 0.02	6.37± 0.04	2.84± 0.07	5.81± 0.08
	FLI1	1.00	0.81± 0.05	0.33± 0.04	0.87± 0.05	0.77± 0.04

	SP1	1.00	1.91± 0.05	3.31± 0.04	0.88± 0.05	0.78± 0.04
	NMYC	1.00	0.95± 0.05	0.79± 0.04	0.90± 0.05	0.91± 0.04
	ZEB1	1.00	0.89± 0.05	0.61± 0.04	0.98± 0.04	0.75± 0.04
Signalling Molecules	PKA	1.00	2.87± 0.09	5.63± 0.04	2.68± 0.08	4.94± 0.01
	PKR (EIF2AK2)	1.00	3.41± 0.03	6.74± 0.02	1.19± 0.01	1.28± 0.09
	PLCB1	1.00	2.58± 0.08	2.59± 0.03	2.42± 0.07	4.82± 0.09
	JUN	1.00	0.90± 0.05	0.72± 0.04	0.86± 0.05	0.75± 0.04

3.4.11 In Vitro Validation of miRNA Expression

To experimentally validate the bioinformatics-based predictions and network analyses, quantitative real-time PCR (qPCR) was performed to assess the expression of **miR-200, miR-345, and miR-577** in U87-MG glioblastoma cells subjected to different treatment conditions. miRNA expression levels were normalized to endogenous U6 small RNA control and expressed as relative fold change compared to untreated controls. Quantitative analysis of miRNA-345-3p expression revealed a significant increase in Kisspeptin-10–treated groups compared to control. Expression levels increased to approximately 1.22-fold in the K10 group ($p < 0.01$) and further to 1.35-fold in the K50 group ($p < 0.001$). Doxorubicin-treated groups (D10 and D50) showed expression levels close to baseline, remaining around 1.05–1.10-fold, with no statistically significant difference compared to control. Expression analysis of miRNA-200c-3p demonstrated a moderate but significant elevation following Kisspeptin-10 treatment. The K10 group showed an increase to approximately 1.08-fold ($p < 0.05$), while the K50 group exhibited a higher expression level of approximately 1.12–1.13-fold ($p < 0.01$) relative to control. In contrast, doxorubicin-treated groups displayed minimal variation, with fold changes remaining near 1.02–1.05, and no significant difference observed. For miRNA-577, Kisspeptin-10 treatment resulted in a significant increase in expression compared to control. The K10 group showed an expression level of approximately 1.12-fold ($p < 0.05$), while the K50 group demonstrated a further increase to approximately 1.17–1.18-fold ($p < 0.01$). Doxorubicin-treated groups exhibited expression levels close to control values, ranging between 1.03 and 1.06-fold, without significant differences (Figure 3.16).

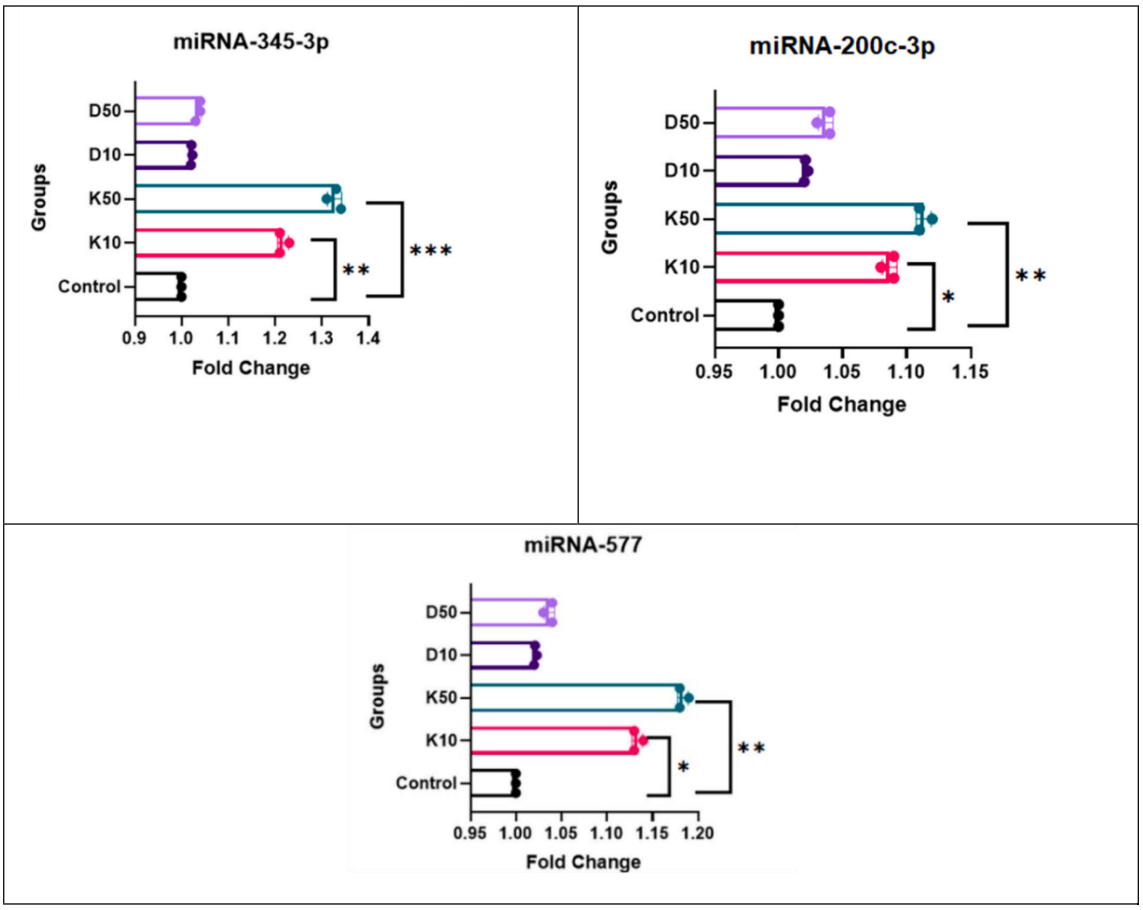

***Figure 3.16**: miRNA Expression analysis of miRNA 345, miRNA 200c-p and miRNA 577 for U87 MG cells.*

3.4.11. Western Blot Analysis

For this purpose, densitometric analysis revealed that the expression level of ZEB1 was significantly down-regulated in K10 (0.24-fold, $p < 0.001$), K50 (0.19-fold, $p < 0.001$), and D10 (0.23-fold, $p < 0.001$) groups compared with the control, while the expression level in the D50 group was moderately, yet significantly, down-regulated (0.64-fold, $p < 0.01$). (Figure 3.16)

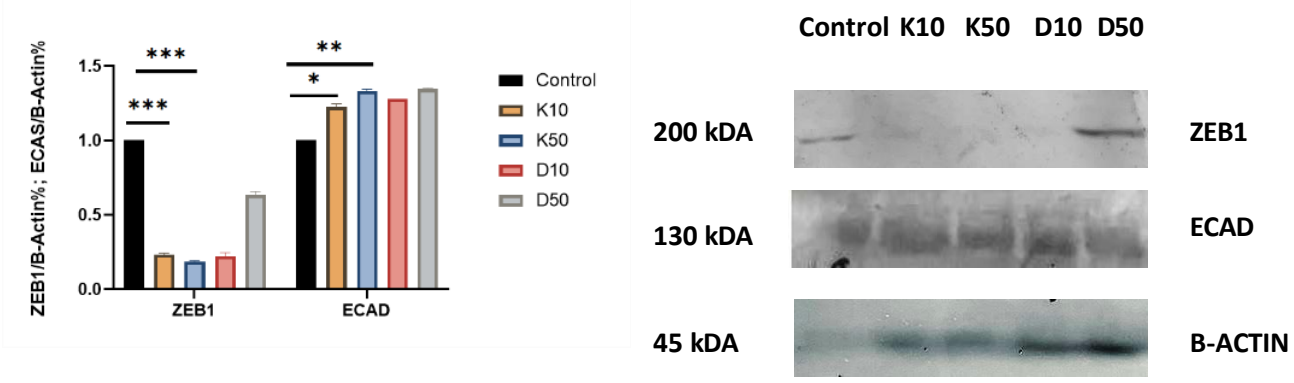

***Figure 3.17:** Protein Expression analysis of ZEB1 and ECAD for U87 MG cells.*

DISCUSSION

Glioblastoma (GB) is one of the most malignant primary tumours in the central nervous system, exhibiting extensive proliferation, diffuse brain invasion, and robust resistance to conventional treatments(Seker-Polat et al., 2022). One among these factors contributing to this aggressive behaviour is that GB cells can perform epithelial-to-mesenchymal transition (EMT)-like events, mediating loss of cell–cell adhesion, increased motility and infiltration into neighbouring neural structures(IWADATE, 2016). Although a growing number of molecular drivers of EMT and invasion in GB have been identified, approaches to target these processes effectively are limited (Aum et al., 2014).Here, we examined the impact of the anti-metastatic peptide Kisspeptin-10 on adhesion, EMT, migration and invasion of U87MG glioblastoma cells, combining in silico network analysis with in vitro functional and molecular corroboration to advance an integrated mechanistic model (Shah et al., 2026).

The present study indicates on how Kisspeptin-10 exerts dose-dependent cytotoxicity and anti-migratory and anti-invasive effects in U87MG cells. Kisspeptin-10 treatment decreased cell viability at nanomolar doses and inhibited wound closure and trans well invasion strikingly (Brown et al., 2019; Liu et al., 2019).These observations are in accordance with previous studies reporting Kisspeptin-induced inhibition of migration and metastasis of prostate, ovarian, breast and melanoma models. Most importantly, we demonstrate that these anti-metastatic actions of Kisspeptin extend to glioblastoma, a tumour type wherein kisspeptin signalling remains relatively unexamined (Cho et al., 2009; Ramaesh et al., 2010).

Glioblastoma is a highly heterogeneous cancer, and the biological outcome of Kisspeptin signalling appears to be context-dependent. Differential expression of *KISS1R*, receptor desensitisation, and internalisation through GRK2/β-arrestin–mediated mechanisms, intracellular signalling bias, as well as microenvironmental signals, may dramatically alter cellular responses to Kisspeptin (Aum et al., 2014; Grech et al., 2020).We previously described pro-invasive actions of Kisspeptin in glioblastoma through biased activation towards PLC-dependent signalling pathways, providing evidence for the double-edged and cell context-dependent nature of *KISS1/KISS1R* signalling (Kim et al., 2020). The apparent discrepancy between those findings and our observations may arise from differences in glioblastoma models, treatment regimens, exposure duration, passage number, or intracellular signalling

state. In our experimental setting, Kisspeptin-10 consistently reduces proliferation and migration and induced transcriptional changes indicative of EMT repression, underscoring the importance of dose–time dynamics and receptor context in determining Kisspeptin's functional outcome (Binder et al., 2018; Zhao et al., 2017). One of the most striking observations in our study was the robust upregulation of E-cadherin (CDH1) following Kisspeptin-10 treatment. E-cadherin is a cornerstone of epithelial integrity, and its loss is widely recognised as a critical initiating event in EMT. Restoration of E-cadherin expression by Kisspeptin has previously been documented in melanoma and breast cancer models, suggesting a conserved mechanism through which Kisspeptin stabilizes cell–cell adhesion and reduces invasion (Bruner & Derksen, 2018; Ramirez Moreno et al., 2021). Our findings indicate that this adhesion-preserving function of Kisspeptin extends to glioblastoma cells, reinforcing epithelial characteristics in a tumour type traditionally considered non-epithelial but highly plastic.(Inda et al., 2014)

Along with the induction of E-cadherin, the mesenchymal identity (N-cadherin), cytoskeletal remodelling (Vimentin) and glioblastoma stemness (CD44) markers were also potently downregulated by Kisspeptin-10. N-cadherin has been reported to promote cell migration and neural invasion in GB, and Vimentin was reported to provide cytoskeletal flexibility and maintain mesenchymal traits (Pearson & Regad, 2017). The downregulation of these markers provides strong molecular evidence for EMT reversal. Notably, CD44, a marker associated with glioblastoma stem-like cells and invasive potential, was also markedly reduced following Kisspeptin-10 treatment. Similar downregulation of CD44 has been reported in ovarian cancer models treated with Kisspeptin, where reduced CD44 expression correlated with decreased invasiveness. The convergence of these findings across multiple tumour types supports the generalizability of Kisspeptin's EMT-suppressive and anti-migratory functions (Loh et al., 2019). Our *in silico* functional enrichment, GO, and KEGG pathway analyses further strengthened these observations. Enrichment of adhesion-related categories such as cadherin binding, adherens junction assembly, focal adhesion, and cytoskeletal organisation aligns closely with the gene expression changes observed experimentally and with previously identified Kisspeptin-regulated pathways (Shah et al., 2026).Additionally, enrichment of neurogenesis and axonogenesis pathways highlights the exploitation of developmental programs by glioblastoma cells to facilitate invasion, consistent with prior reports. Kisspeptin-10–mediated modulation of these pathways suggests a potential interface between adhesion regulation and neurodevelopmental signalling in GB, raising intriguing possibilities for broader

regulatory roles of Kisspeptin in Glioblastoma (DeCordova et al., 2020). At the post-transcriptional level, our miRNA–mRNA network analysis and in vitro validation identified miR-200, miR-345, and miR-577 as central regulatory hubs induced by Kisspeptin-10. miR-200 is a well-established suppressor of EMT and directly targets transcriptional regulators such as ZEB1, providing a mechanistic basis for the observed upregulation of E-cadherin and repression of mesenchymal markers(Y. Zhang et al., 2019). miR-345 and miR-577 further contribute by regulating apoptotic and survival pathways, thereby coupling EMT suppression with apoptotic sensitisation. This coordinated miRNA induction suggests that Kisspeptin-10 does not merely inhibit invasion mechanically but reprograms glioblastoma cells at multiple regulatory layers (Drápela et al., 2020a).

Our transcription factor studies indicated even further levels of control. Kisspeptin-10 downregulated HDAC2 (in line with epigenetic relaxation permissive for differentiation and apoptosis) as well as GATA2 and CDX2, transcription factors implicated in epithelial differentiation and maintenance of the lineage (Shan et al., 2017). By contrast, the potential driver of invasion and proliferation, transcription factors FLI1, JUN, SP1, and NMYC was downregulated. This coordinated transcriptional reprogramming probably enhances the shift in phenotypic potential toward these less invasive, more differentiated cells. Although correlations with E-cadherin and CD44 are not statistically significant, the directionality of these associations remained consistent with our *in vitro* results (Ponta et al., 2003). This suggests that Kisspeptin's regulatory influence on EMT markers may be more evident at the functional and cellular level than in bulk transcriptomic analyses, which are confounded by tumour heterogeneity and stromal contributions (Iseki et al., 2017).

Overall, our study confirms and extends previous observations in breast, ovarian, melanoma and prostate cancer model systems showing that Kisspeptin-10 inhibits migration, invasion, as well as EMT-like processes in glioblastoma. Through combining miRNA-mediated regulation, transcription factor reprogramming, and epigenetic modulation with functional repression of invasion, we reveal an integrated mechanistic scenario underlying Kisspeptin's anti-invasive property in GB (Shah et al., 2026a). These results further contribute to the accumulating evidence that reinforces Kisspeptin-10 as a key regulator of tumour plasticity, adhesion dynamics and mesenchymal phenotypes and gives new possibilities for therapeutic intervention in glioblastoma.

CONCLUSION

In the present study, we systematically elucidated the molecular and functional impact of **exogenous Kisspeptin-10** on glioblastoma by integrating transcriptomic analyses, regulatory network modelling, *and in vitro* validation. The molecular composite framework that we present here, and that is summarised in the final schematic model, highlights the potential of the *KISS1/KISS1R* axis as a novel target for modulating tumour plasticity, adhesion mechanics, and survival mechanisms in glioblastoma. Taken together, these data support further in vivo testing and investigation of Kp-10 as a novel multi-targeted therapeutic approach for glioblastoma.

Similarly, in ovarian cancer key oncogenic features observed in glioblastoma, including enhanced invasiveness, EMT activation, transcriptional dysregulation, and apoptotic resistance, supporting the exploration of conserved regulatory mechanisms. Therefore, the next chapter evaluates the role of Kisspeptin-10 in SKOV-3 cells to determine whether its EMT-suppressive and pro-apoptotic effects are conserved across epithelial cancer.

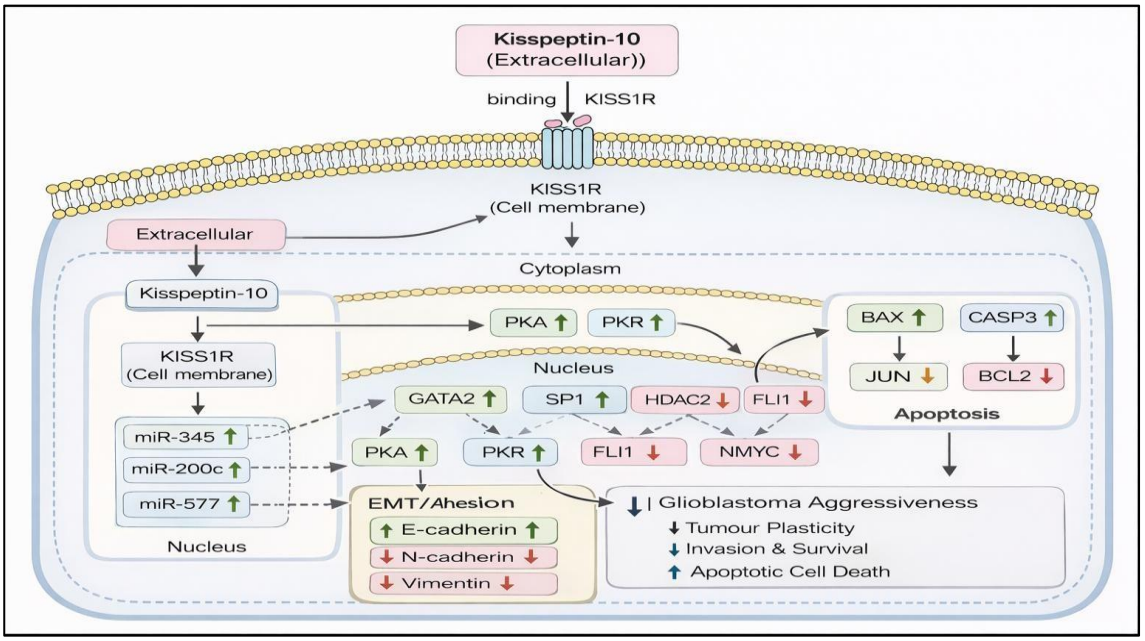

Figure 3.16: *Conclusion image depicting the overall role of exogenous Kisspeptin-10 treatment on U87MG cells and its associated markers*